Biochar and enhanced phosphate capture: Mapping mechanisms to functional properties

Biochar and enhanced phosphate capture: mapping mechanisms to functional properties

Jessica Shepherd[1,2*], Stephen Joseph[3,4], Saran Sohi[1,2], Kate Heal[1]

Affiliations

1) School of GeoSciences, University of Edinburgh, Alexander Crum Brown Road, Edinburgh, UK EH9 3FF

2) UK Biochar Research Centre, University of Edinburgh, Alexander Crum Brown Road, Edinburgh, UK EH9 3FF

3) School of Environmental and Life Sciences, University of Newcastle, Office C325, Chemistry, Callaghan, New South Wales 2308, Australia

4) School of Materials Science and Engineering, University of New South Wales, Kensington, NSW, Australia 2052

*Corresponding author

Abstract

A multi-technique analysis was performed on a range of biochar materials derived from secondary organic resources and aimed at sustainable recovery and re-use of wastewater phosphorus (P). Our purpose was to identify mechanisms of P capture in biochar and thereby inform its future optimisation as a sustainable P fertiliser. The biochar feedstock comprised pellets of anaerobically digested sewage sludge (PAD) or pellets of the same blended in the ratio 9:1 with ochre sourced from minewater treatment (POCAD), components which have limited alternative economic value. In the present study the feedstocks were pyrolysed at two highest treatment temperatures of 450 and 550°C. Each of the resulting biochars were repeatedly exposed to a 20 mg l^{-1} PO_4-P solution, to produce a parallel set of P-exposed biochars. Biochar exterior and/or interior surfaces were quantitatively characterised using laser-ablation (LA) ICP-MS, X-ray diffraction, X-ray photo-electron spectroscopy (XPS) and scanning electron microscopy coupled with energy dispersive X-ray. The results highlighted the general importance of Fe minerals in P capture. XPS analysis of POCAD550 indicated lower oxidation state Fe2p3 bonding compared to POCAD450, and LA-ICP-MS indicated stronger covariation of Fe and S, even after P exposure. This suggests that low-solubility Fe/S compounds are formed during pyrolysis, are affected by process parameters and impact on P capture. Other data suggested subsidiary roles for aluminium, calcium and silicon. Overall, our analyses suggest that a range of mechanisms for P capture are concurrently active in biochar. We highlighted the potential to manipulate these through choice of form and composition of feedstock as well as pyrolysis processing, so that biochar may be increasingly tailored towards specific functionality.

Keywords

Phosphorus capture mechanisms; Biochar; Anaerobically digested sewage sludge; Ochre; Phosphorus recycling; Wastewater treatment

1 Introduction

Freshwater and coastal ecosystems are at a high risk of damage caused by excess flows of phosphate from land application and wastewater (Steffen et al., 2015). Concurrently there is growing interest in the research, innovation and regulatory sectors to improve the recovery and recycling of phosphate as agricultural fertiliser in response to predicted future mineral phosphorus (P) scarcity (Reijnders, 2014). Traditional flocculation techniques may not be effective for limiting P concentrations in wastewater discharges to watercourses to reduce the risk of environmental damage to acceptable levels, for example the 0.1 mg l^{-1} level proposed by Greenop and Wentworth (2014). Therefore, alternative tertiary treatment methods are required, such as constructed wetlands increasingly utilised in smaller wastewater treatment plants (WWTPs), using combinations of plant, soil, and reactive materials to remove phosphate and nitrate to prevent environmental damage downstream.

In order to recycle P from wastewater it is important that the materials used to recover P are economic and the underlying mechanisms of P capture well understood. Low-cost, bulk filter materials investigated to date include ochre, zeolite and blast furnace slags (Cucarella et al., 2008; Dobbie et al., 2009; Drizo et al., 2006). The main mechanisms of P capture in these systems are either chemisorption and precipitation by Fe or Al (oxy)hydroxides, or precipitation with Ca (Arai and Sparks, 2001; Sakadevan and Bavor, 1998). Activated carbons have also been developed for this purpose (Wang et

al., 2012), but the manufacture of these materials is more expensive than the direct recycling of secondary organic resources. A number of biochar materials, because of their similarities to activated carbon, have also been investigated. Biochars produced from anaerobically digested sugar beet tailings, digested sewage sludge and mallee tree (*Eucalyptus polybractea*) have all been shown to have phosphate capture functionality (Shepherd et al., 2016; Yao et al., 2011; Zhang et al., 2016), but most studies have involved either feedstock pre-treatment (Chen et al., 2011; Shepherd et al., 2016; Yao et al., 2011; Zhang et al., 2013, 2012) or post-treatment of the biochar (Li et al., 2016; Park et al., 2015; Ren et al., 2015; Zhang et al., 2016) to increase porosity and enrich the biochar with Mg, Al or Fe oxides.

Although many P sorption studies are reported in the literature, there is still no definitive model for biochar–phosphate interactions. Adding to the complexity of the system, many biochars have been shown to release, rather than capture phosphate into water and/or phosphate solutions (Angst and Sohi, 2013; Morales et al., 2013; Schneider and Haderlein, 2016). It has been suggested that phosphate may react with hydroxyl and carboxyl groups on the biochar surface (Laird and Rogovska, 2015) but such a reaction can only occur in the environment under extreme conditions or, in the case of biota, with the assistance of specialised enzymes (Gull et al., 2014). It is possible that the various phosphate anion species ($H_2PO_4^-$, HPO_4^{2-}, PO_4^{3-}) interact with C surfaces through hydrogen bonding and cation-mediated outer-sphere electrostatic interactions. These are weak compared to inner-sphere chemisorption and precipitation reactions which would occur with minerals, and thus are unlikely to be long-lived, unless in a relatively static system such as undisturbed soil. It has been suggested that adsorption of P by biochar will be dependent on the concentration and accessibility of

cations in the biochar ash fraction (Streubel et al., 2012). This is supported by reports of low affinity for P of low-ash biochar in aqueous solution (Hale et al., 2013; Morales et al., 2013; Yao et al., 2012). Even in biochar that has not been chemically modified, the identified mechanisms of P capture have been related to a native mineral ("ash") phase (Yao et al., 2011; Zhang et al., 2016), rather than functional carbon groups. The focus of subsequent optimisation of P capture properties has thus been on increasing the concentration and effectiveness of mineral phases on biochar surfaces. This can be likened to the research and development of activated carbon, where the activation step for improving P capture properties usually involves the addition of a metal reagent such as Fe or Zn (Bhatnagar and Sillanpää, 2011; Namasivayam and Sangeetha, 2004; Wang et al., 2012). Drawing on the general principles of coordination chemistry suggested by Streubel et al. (2012), we support a dominant role for minerals, but emphasise the mineral-carbon interface. The specific role of Fe, Al, Ca and Mg will vary with pH, as has been widely documented (Barrow, 1983; Goldberg and Sposito, 1985; Parfitt and Russell, 1977; Parfitt, 1989; Parfitt et al., 1975; Reddy et al., 1999; Sibrell et al., 2009; Torrent et al., 1992). This needs to be understood in the context of interface interactions.

In a previous study, we tested biochars made from a novel mix of anaerobically digested sewage sludge and ochre (Shepherd et al., 2016). The mix captured a greater amount of P from solution on a mass basis than activated carbon, ochre, or biochar from digested sludge only. To investigate the mechanisms underlying the P-capture function of that biochar we initiated the present study, with the overall goal of furthering the practical design of P capture materials in general. Consistent with this more practical context, we prepared new biochars using the original ingredients but pelletised before pyrolysis. We also used lower ochre content in mixed feedstock, namely 1:9 rather than 1:1 mass ratio. The surface properties were studied before and after exposure to aqueous P using a

range of spectroscopic and visualisation techniques. Our overarching hypothesis was that P capture would be driven predominantly by mineral associations on surfaces and less by functional carbon groups.

2 Methods

A summary of the materials, procedures and analyses used in this study and their respective aims is given in Table 1. The biochars collectively encompass the range of ochre (and therefore Fe), ash constituents and carbon components that allows the relative contribution to P capture to be assessed. Characterisation was undertaken on sub-samples with and without prior exposure to aqueous P solution, and of exterior and/or interior surfaces of individual particles or pellets. Different characterisation techniques covered different physical surface areas or surface thickness (i.e. sample volume); they also provide information at different levels of detail, e.g. elemental composition, functional groups, or oxidation state.

2.1 Biochars

2.1.1 Non-pelletised biochars

Biochars from non-pelletised feedstock were from the previous study (Shepherd et al., 2016). They were produced in a small batch pyrolysis system at highest treatment temperatures (HTTs) of 450 and 550°C. The feedstocks were anaerobically digested sewage sludge (giving biochars AD450 and AD550) and the same sludge mixed with ochre at a dry-mass ratio of 1:1 (giving biochars OCAD450 and OCAD550). These relatively low HTTs were originally chosen so as to produce biochar with reactive sites potentially related to carbon functional groups (Downie et al., 2009).

139 *Table 1: Summary of the materials, analyses and their aims described in this study. First generation biochar materials AD450, AD550,*
140 *OCAD450, OCAD550 as well as ochre and activated carbon were characterised in Shepherd et al. (2016) and are indicated in italics. Elemental*
141 *concentrations of these materials determined previously by modified dry ashing/ICP-OES are outlined in Supplementary Information Tables S1*
142 *and S2. The pelletised materials were produced for this study and were characterised by the techniques listed above.*

Material	Analyses							
	P capture and Release	**Correlation of P capture/element concentrations**	**Modified dry ashing/ICP-OES**	**pH and EC**	**XRD**	**XPS**	**LA-ICP-MS**	**SEM-EDX**
AD450	✓*(previous work)*	✓	✓*(previous work)*	✓*(previous work)*	-	-	-	-
AD550	✓*(previous work)*	✓	✓*(previous work)*	✓*(previous work)*	-	-	-	-
OCAD450	✓*(previous work)*	✓	✓*(previous work)*	✓*(previous work)*	-	-	-	-
OCAD550	✓*(previous work)*	✓	✓*(previous work)*	✓*(previous work)*	-	-	-	-
Ochre	✓*(previous work)*	✓	✓*(previous work)*	✓*(previous work)*	-	-	-	-
Activated carbon	✓*(previous work)*	✓	✓*(previous work)*	✓*(previous work)*	-	-	-	-
PAD450	✓ (capture only)	-	✓	✓	✓	-	-	✓
PAD550	✓ (capture only)	-	✓	✓	✓	-	-	✓
POCAD450	✓ (capture only)	-	✓	✓	✓	✓	✓	✓
POCAD550	✓ (capture only)	-	✓	✓	✓	✓	✓	✓
EPAD450	N/A	N/A	-	-	✓	-	-	✓
EPAD550	N/A	N/A	-	-	✓	-	-	✓
EPOCAD450	N/A	N/A	-	-	✓	✓	✓	✓
EPOCAD550	N/A	N/A	-	-	✓	-	✓	✓
Mechanistic and chemical information obtained	Determination of P capture/release characteristics	Effect of elemental composition on P capture and release	Effect of feedstock, processing and/or pyrolysis conditions and pyrolysis HTT on elemental composition	Effect of feedstock, processing and/or pyrolysis conditions and pyrolysis HTT on pH and EC	Effect of feedstock, pyrolysis HTT and P exposure on mineral phases	Effect of P exposure on surface and whole properties	Effect of pyrolysis HTT and P exposure on surface properties	Effect of feedstock, pyrolysis HTT and P exposure on surface properties
Biochar nomenclature	AD – Anaerobically digested sewage sludge OCAD – 50% Minto ochre and AD mixture (pre-pyrolysis) PAD – Pelletised Anaerobically digested sewage sludge POCAD – Pelletised 10% Minto ochre and AD mixture (pre-pyrolysis)				EPAD – P exposed PAD biochar EPOCAD – P exposed POCAD biochar 450 – 450°C highest treatment temperature (HTT) for pyrolysis 550 – 550°C highest treatment temperature (HTT) for pyrolysis			

143 **2.1.2 Pelletised biochars**

144 Biochars were made from pelletised feedstocks using a bench-scale continuous
145 pyrolysis unit. It is more practical to pelletise feedstock than biochar; screw-feeders
146 used in scalable, continuous flow pyrolysis systems also perform best with feedstock in
147 pelletised form. The digested sewage sludge and ochre were sourced from the same
148 locations as in the previous study. Anaerobically digested sewage sludge (50 kg wet
149 mass) was sampled from the Newbridge WWTP (Edinburgh, Scotland) and oven dried.
150 Ochre was obtained from the Minto minewater treatment plant (Fife, Scotland) and
151 sieved to < 1 mm. Pellets were prepared from the sludge and/or ochre and a
152 lignocellulose binder agent in the ratios 89.1:9.9:1.0 and 99.0:0:1.0. The mixtures were
153 passed through a die to form pellets approximately 0.5 cm diam. × 2 cm in length. The
154 pellets were pyrolysed at the UK Biochar Research Centre (UKBRC) using the bench-
155 scale continuous flow unit described previously (Buss et al., 2016a). The HTTs used in
156 the previous study (Shepherd et al., 2016) were used to produce the four new biochar
157 materials: PAD450, PAD550, POCAD450 and POCAD550.
158

159 **2.1.3 P–exposed pelletised biochars**

160 To investigate the mechanisms of P capture on biochar surfaces, pelletised biochars
161 defined above were exposed to aqueous P using a MOPS-buffered (3-(*N*-morpholino)
162 propanesulfonic acid, Sigma Aldrich, St Louis, MI) K_2HPO_4 solution containing
163 20 mg P l^{-1}, following the procedure described previously (Shepherd et al., 2016)
164 modified as described here. Each biochar (30 g, PAD450, PAD550, POCAD450 and
165 POCAD550) was used to provide representative particles of the physically
166 heterogeneous samples, selecting only particles of diameter 0.25–15 mm. The P
167 solution was added in a 1:20 solid to liquid ratio (m/v) and shaken with the biochar for

24 h. After this time the solution was poured off from the biochar and replaced with fresh P solution. This was repeated for 6 days to ensure sufficient uptake of P on the external surfaces of the biochar to analyse using the chosen techniques. At the end of each 24 h treatment two samples of the solution were analysed colorimetrically (Auto Analyser III, Bran & Luebbe, Norderstedt, Germany) to determine the amount of P captured by the biochars. The P-exposed samples were designated EPAD450, EPAD550, EPOCAD450 and EPOCAD550.

2.2 Characterisation

2.2.1 pH – pelletised biochars

To provide insights on surface protonation of pelletised biochars, the pH of crushed samples was determined in duplicates for PAD450, PAD550, POCAD450 and POCAD550, in DI water using the method recommended by the International Biochar Initiative (IBI).(IBI, 2012)

2.2.2 P capture and release – non-pelletised biochars

P-capture and release dynamics of the non-pelletised biochars (AD450, AD550, OCAD450 and OCAD550) were described and reported in the previous study (Shepherd et al., 2016). It is the statistical analysis of the results in the light of new characterisation data that is the main focus of the present study. Briefly, replicate (n = 4) 1.0 g samples of each biochar, the ochre and an activated carbon (Sigma Aldrich, St Louis, MI) were repeatedly exposed for 24 h repeated over 5 days to 20 ml solutions of either 20 or 800 mg l^{-1} P (from K_2HPO_4, Sigma Aldrich, St Louis, Missouri, USA) buffered at pH 7 using MOPS and $NaNO_3$ as a background electrolyte. To test the

192 release of the captured P, the P-enriched materials were then exposed to pH 7 MOPS-
193 buffered deionised (DI) water for 24 h repeatedly over 4 days.
194
195 **2.2.3 Bulk elemental composition – pelletised and non-pelletised biochars, ochre**
196 **and activated carbon**
197 Samples were digested prior to ICP-OES analysis using the modified dry ashing method
198 (Enders and Lehmann, 2012), as per published modifications (Buss et al., 2016b;
199 Shepherd et al., 2016). Briefly, 0.5 g samples were taken from sub-sampled and crushed
200 materials, ashed in a muffle furnace then digested in HNO_3 and HCl. The materials and
201 blanks were digested in triplicate and ICP-OES elemental quantification was performed
202 using a Perkin Elmer Optima 5300DV instrument (Waltham, USA). Most elements
203 were analysed in axial mode, except for Al, Ca, Fe, K, Mg and Na, which were present
204 in sufficient concentrations to necessitate the use of radial mode. Standards were run
205 with each analysis session for calibration and to check the accuracy of measurements
206 over the time of the sample run. The limit of detection for each element was determined
207 using an existing method (Buss et al., 2016b).
208
209 **2.2.4 X-ray diffraction (XRD) – pelletised biochars**
210 Cobalt Kα XRD was performed in duplicate on PAD450, PAD550, POCAD450,
211 POCAD550, EPAD450, EPAD550, EPOCAD450 and EPOCAD550 using an
212 Empyrean thin-film XRD (PANalytical, Almelo, the Netherlands). Analyses were
213 initially attempted using standard Cu Kα XRD, but confounded by the large background
214 signal from amorphous carbon phases.
215
216 **2.2.5 X-ray photoelectron spectroscopy (XPS) – pelletised biochars**

Surface layer functional groups and elemental composition was examined for one randomly sampled pellet fragment of POCAD450, EPOCAD450 and POCAD550. Mono-chromated Al Kα XPS was applied using an ESCALAB250Xi instrument (Thermo Scientific, Waltham, MA). The analysis parameters were as follows: 1486.68 eV photon energy, 150 W power and spot size of 500 μm. The core level binding energies (BEs) were aligned with C1s peak BE of 285.0 eV. Data were analysed with Avantage software (Thermo Scientific, Waltham, MA). The surfaces of POCAD450 and EPOCAD450 pellets were analysed to identify differences in properties before and after P exposure, respectively. Surfaces of POCAD550 were also analysed to identify whether pyrolysis HTT had an effect on surface composition in these biochars. To gain an insight as to the effect on pellet size on the utilised capacity for P interaction measurements were also conducted on interior surfaces of the analysed POCAD and EPOCAD, exposed by crushing the pellet.

2.2.6 Laser ablation-ICP-MS – pelletised biochars

To study the relationship between P and other elements on the surface of P-exposed and non-treated biochar to a depth of 5 μm, elemental analysis by laser ablation (LA) ICP-MS was used. The analysis was applied to a randomly selected pellet of each of POCAD450, POCAD550, EPOCAD450 and EPOCAD550 using a NWR213 Laser Ablation unit (ESI New Wave, Portland, OR) coupled to a NexION 300D ICP-MS (Perkin Elmer, Waltham, MA). Laser ablation parameters were as follows: wavelength 213 nm, repetition frequency 10 Hz, laser energy density 0.48 J cm^{-2} (at 30%), spot size 110 μm and scan speed 20 μm s^{-1}. ICP-MS was performed at Rf power of 1150 W, helium gas flow rate of 0.8 l min^{-1}, argon gas flow rate of 0.6 l min^{-1}, in peak hopping scan mode and with a dwell time of 0.05 s. NIST610 and NIST612 glass standards were

used to estimate the elemental concentrations of the biochar obtained in three separate 2 mm line scans for each pellet (resulting in between 219 and 223 sample locations for each pellet).

2.2.7 Scanning electron microscopy with energy-dispersive X-ray spectroscopy (SEM-EDX)

SEM-EDX analyses were performed on all P-exposed and non-exposed biochars (PAD450, PAD550, POCAD450, POCAD550, EPAD450, EPAD550, EPOCAD450 and EPOCAD550) to a depth of approximately 6 µm. Data was gathered using Nova Nano SEM 230 and 450 field-emission scanning electron microscopes (FEI, Hillsboro, OR), each configured with a Bruker silicon drift detector energy dispersion X-ray spectrometer (Bruker, Billerica, MA), as well a Sigma SEM (Zeiss, Jena, Germany). Samples were sputter coated with chromium prior to analysis. The resolution of EDX scans was 6 µm. To encompass as many P phases as possible, the whole region was quantified; many P phases have a dimension in the µm range. Elemental mapping provided by EDX was used to visualise the association of P and other elements in support of the other analyses.

2.3 Statistical analysis

2.3.1 Correlation of biochar element concentration and P capture and release – non-pelletised biochars

To identify whether specific elements were associated with P capture or release, mean P capture and release results (n = 6) were correlated against the concentration of 19 elements in AD450, AD550, OCAD450, OCAD550, ochre and activated carbon determined as described in 2.2.3. The cumulative results for 1 and 5 days x 20 mg l^{-1} P

repeated exposure and 1 and 4 days x treatments for P release as described in section 2.2.2 were used. Pearson's product-moment correlation coefficients were calculated since all data were found to be normally distributed by the Shapiro-Wilk test. Where element concentrations were below the limit of detection for two or more of the materials (i.e. resulting in $n < 4$), the element was excluded from the analysis. RStudio (RStudio Team, 2015) was used for all statistical analyses, with significance indicated by $p < 0.05$.

2.3.2 Analysis of Laser ablation ICP-MS results

Correlation analysis between P and other elements measured by LA-ICP-MS was performed using the approach described in 2.3.1, with Spearman's rho calculated where one or both sets of data were not normally distributed. To further interpret elemental composition on biochar surfaces, we applied Principal Component Analysis (PCA) to the results for each sample location using the prcomp function in RStudio (RStudio Team, 2015) with data centring, scaling and specifying a tolerance of 0.3 to filter out noise and thereby limit the number of identified principal components. PCA provides insights into elemental clustering as well as the localisation of P on sample surfaces before and after exposure to P solution.

3 Results

3.1 Bulk properties

3.1.1 Elemental composition

The lower content of ochre in the POCAD feedstock compared to OCAD (10 vs 50%) explained some differences in nutrient concentrations between PAD and POCAD (Table 2) compared to their non-pelletised analogues (AD and OCAD). In general, the

292 non-pelletised biochars appeared to show greater elemental loss on a mass basis,
293 compared to their feedstocks, than for the pelletised biochars (See Supplementary
294 Tables 1 and 2 for more detail). Calcium and P present in the feedstocks was retained to
295 a higher extent in the pelletised biochars, suggesting that either pelletisation and/or the
296 continuous flow bench scale pyrolysis process provides conditions less conducive for
297 volatilisation of Ca and P than small scale batch pyrolysis.
298
299 The main difference between the PAD and POCAD biochars was in the concentration
300 of Fe, reflecting feedstock composition (see Table 3). The incorporation of 10% ochre
301 (dry weight) to the feedstock resulted in a Fe concentration in POCAD twice that of
302 PAD. Despite similar concentrations in PAD and POCAD feedstocks, POCAD
303 contained relatively less Cr than PAD at both HTTs (24.9 ± 0.880 and 21.1 ± 1.16 mg g^{-1}
304 for POCAD vs 33.8 ± 1.25 and 30.1 ± 0.538 mg g^{-1} for PAD) (mean ± 1 standard
305 deviation, n = 3). Compared to the non-pelletised biochars, the PAD and POCAD
306 biochars contained more Al, Cr, Cu, Mo, Na, Ni and Zn, but less B and Co. The lower
307 Co concentration reflects a lower concentration in the feedstock, but this is not the case
308 for B, which may have also been lost during digestion in the modified dry ashing
309 process. The concentrations of Mo and Na in the pelletised feedstocks are higher than in
310 non-pelletised, explaining part of the difference in concentration in the biochars. In
311 addition, there is considerably more Cr, Cu and Zn in POCAD than OCAD, probably
312 from contamination of feedstock during the pelletisation process. Overall, the data
313 indicate that pelletisation and/or continuous flow pyrolysis favours greater retention of
314 some elements in biochar. The pH of the pelletised biochars ranged from 7.39 to 8.25,
315 which is slightly higher than for the non-pelletised analogues. This is likely to be related
316 to the relative retention of salts discussed above.

317 *Table 2: Mean nutrient concentrations (n=3) of the materials as determined by ICP-OES of sample digests expressed in g kg^{-1} ± 1 standard*

318 *deviation. See Table 1 for sample nomenclature.*

319

	PAD	Ochre	POCAD	PAD450	POCAD450	PAD550	POCAD550
Yield %	-	-	-	**29.4**	**38.7**	**37.9**	**38.0**
pH (n=2)	-	**7.9** ± 0.014	-	**7.49 ± 0.02**	**7.39 ± 0.05**	**8.25 ± 0.08**	**7.85 ± 0.03**
EC (µS cm^{-1}) (n=2)	-	**518** ± 20	-	**TBC**	**TBC**	**TBC**	**TBC**
			Nutrients (g kg^{-1}) n=3				
Ca	28.7 ± 0.569	18.8 ± 0.438	28.8 ± 0.400	59.9 ± 1.98	58.1 ± 0.534	62.0 ± 1.06	53.9 ± 1.08
K	2.53 ± 3.99×10^{-2}	0.349 ± 4.76×10^{-2}	2.10 ± 2.69×10^{-2}	5.09 ± 0.142	4.59 ± 6.75×10^{-2}	5.51 ± 6.61×10^{-2}	4.20 ± 0.125
Mg	5.12 ± 7.96×10^{-2}	3.03 ± 5.88×10^{-2}	5.09 ± 5.79×10^{-2}	10.4 ± 0.281	10.5 ± 0.107	10.8 ± 0.138	9.52 ± 0.209
Mn	0.142 ± 0.149×10^{-2}	0.891 ± 5.33×10^{-3}	0.183 ± 0.278×10^{-2}	0.327 ± 0.881×10^{-2}	0.373 ± 0.528×10^{-2}	0.336 ± 0.969×10^{-2}	0.357 ± 0.856×10^{-2}
P	52.1 ± 9.62×10^{-2}	1.92 ± 0.134	51.5 ± 0.561	109 ± 3.08	103 ± 1.95	114 ± 1.19	98.7 ± 1.73
S	9.82 ± 0.425	3.32 ± 0.121	8.81 ± 0.160	16.8 ± 0.406	18.1 ± 0.279	16.3 ± 0.203	16.6 ± 0.217

320 *Table 3: Mean potentially toxic element concentrations (n=3) of the materials as determined by ICP-OES of sample digests expressed in mg kg^{-1}*

321 *± 1 standard deviation. See Table 1 for sample nomenclature.*

	PAD	Ochre	POCAD	PAD450	POCAD450	PAD550	POCAD550
Al	$23.6\times10^3 \pm 121$	$2.09\times10^3 \pm 227$	$22.7\times10^3 \pm 151$	$46.5\times10^3 \pm 953$	$46.6\times10^3 \pm 354$	$49.5\times10^3 \pm 666$	$43.4\times10^3 \pm 1130$
As	< 0.72	< 0.72	< 0.72	< 0.72	< 0.72	< 0.72	< 0.72
B	$9.26 \pm 9.28\times10^{-2}$	43.8 ± 6.09	15.3 ± 3.46	18.6 ± 0.428	19.8 ± 1.49	18.0 ± 0.159	16.1 ± 0.407
Cd	$0.281 \pm 1.77\times10^{-2}$	< 0.04	< 0.04	$1.77 \pm 4.33\times10^{-2}$	$0.169 \pm 1.05\times10^{-2}$	$1.15 \pm 9.33\times10^{-2}$	$0.322 \pm 8.54\times10^{-2}$
Co	2.94 ± 0.264	$9.65 \pm 5.98\times10^{-2}$	$3.10 \pm 5.52\times10^{-2}$	6.05 ± 0.139	6.71 ± 0.119	6.30 ± 0.167	6.10 ± 0.190
Cr	11.8 ± 0.233	< 0.49	10.6 ± 0.674	33.8 ± 1.25	24.9 ± 0.880	30.1 ± 0.538	21.1 ± 1.16
Cu	44.0 ± 1.18	< 0.06	39.1 ± 0.572	110 ± 1.54	103 ± 2.10	112 ± 7.67	98.9 ± 3.70
Fe	$38.9\times10^3 \pm 719$	$520\times10^3 \pm 7.44\times10^3$	$77.0\times10^3 \pm 2.51\times10^3$	$80.8\times10^3 \pm 2.93\times10^3$	$130\times10^3 \pm 2.00\times10^3$	$84.5\times10^3 \pm 1.53\times10^3$	$130\times10^3 \pm 1.92\times10^3$
Mo	10.9 ± 0.556	< 0.21	12.5 ± 0.942	21.9 ± 0.459	26.7 ± 0.620	23.8 ± 0.756	24.3 ± 0.287
Na	$5.11\times10^3 \pm 274$	$1.86\times10^2 \pm 30.3$	$1.33\times10^3 \pm 44.4$	$9.90\times10^3 \pm 219$	$5.23\times10^3 \pm 48.5$	$10.5\times10^3 \pm 208$	$3.75\times10^3 \pm 171$
Ni	7.14 ± 0.549	$5.90 \pm 7.79\times10^{-2}$	7.23 ± 0.178	29.4 ± 0.895	$23.0 \pm 9.81\times10^{-2}$	26.3 ± 0.889	18.8 ± 0.420
Pb	11.8 ± 0.362	10.1 ± 0.824	13.2 ± 1.77	31.9 ± 4.23	25.1 ± 0.351	29.8 ± 0.771	28.3 ± 3.72
Zn	360 ± 4.75	60.6 ± 0.985	350 ± 2.71	787 ± 9.68	746 ± 6.50	825 ± 15.8	706 ± 12.4

3.1.2 Phosphorus exposure of the pelletised biochars

Repeated exposure of biochars to 20 mg P l^{-1} MOPS-buffered solution resulted in P capture of 0.57 ± 0.26 mg P g^{-1} for PAD450 (mean ± 1 standard deviation, n = 2), 0.70 ± 0.40 mg P g^{-1} for PAD550, 0.95 ± 0.18 mg P g^{-1} for POCAD450 and 0.95 ± 0.23 mg P g^{-1} for POCAD550. The P capture by non-pelletised biochars AD and OCAD(Shepherd et al., 2016) were higher: 0.99 ± 9.3×10^{-3} mg P g^{-1} to 1.3 ± 4.7×10^{-3} mg P g^{-1}. This may be attributed to the larger size of analysed pellet fragments (0.25–15 mm) compared to crushed particles (0.5–1.0 mm) i.e. a surface area effect.

3.1.3 Elemental associations in P capture and release for non-pelletised biochars

The significant correlations between P capture and release and bulk element concentrations are shown for AD450, AD550, OCAD450, OCAD550, ochre and activated carbon in Table 4. After 1 day (1 x 24 h) exposure to a 20 mg P l^{-1} solution, P capture from solution was correlated negatively and strongly significantly with biochar Al, Cu, K, Na and Zn concentration. After 5 days (5 x 24 h) of exposure only Pb was significantly correlated (negatively), although Pb concentration of the materials was also very low (< 3.2 × 10^{-3} g kg^{-1}). After 5 days, P capture was positively and strongly significantly correlated with Fe, which was present in biochar at 44.6–451 g kg^{-1}.

In terms of P release following P exposure, after 1 day shaking in MOPS-buffered pH 7 DI water, P release was significantly negatively correlated with Fe, suggesting that higher Fe content is associated with lower solubility of captured P at pH 7. After 4 days the negative correlation with Fe was no longer significant, but P release was significantly positively correlated with both initial biochar Cu and Na concentration,

indicating that these elements may be present in P compounds of greater solubility after P capture.

Table 4: Pearson's product-moment correlation coefficients for elements where a statistically significant correlation between elemental concentration and P capture or P release was determined (n = 6) at the start or end of the experiments for the first generation materials (AD450, OCAD450, AD550, OCAD550, ochre and activated carbon) using a 20 mg P l^{-1} solution reported in Shepherd et al. (2016). * *= p < 0.05,* ** *= p < 0.01,* *** *= p < 0.001*

	P capture		**P release**	
	Day 1	**Day 5**	**Day 1**	**Day 4**
Al	-0.886*	-0.412	-0.194	0.0916
Cu	-0.961**	-0.478	0.642	0.860*
Fe	0.605	0.878*	-0.858*	-0.740
K	-0.850*	0.465	0.528	0.748
Mn	0.194	0.711	-0.609	-0.382
Na	-0.967**	-0.521	0.664	0.879*
Pb	-0.292	-0.887*	0.786	0.536
Zn	-0.854*	-0.358	0.487	0.730

3.1.4 Mineral phases identified by X-ray diffraction

Due to the presence of amorphous C in the pelletised biochars, few mineral elements were identified, even using the Co method (Table 5). The analysed biochars all contained SiO_2 (quartz). Other detectable minerals were mostly complex silicates containing different combinations of Al, Ca, K, Mg, Mn and Na. The only phosphate-containing mineral detected was Al phosphate in EPOCAD450. Interestingly, no iron minerals were identified, indicating that Fe is either amorphous or present in a diversity of crystalline forms at very low individual concentrations.

372 *Table 5: Minerals detected in the pelletised biochars using Co Kα X-ray diffraction. See*
373 *Table 1 for sample nomenclature.*

Sample	Minerals detected
PAD450	SiO_2 $Na_2S_2O_3$ $K_{1.2}Al_4Si_8O_{20}(OH)_4.4H_2O$ $Na_3Mg_3Ca_5Al_{19}Si_{117}O_{272}$
PAD550	SiO_2 $Na_2S_2O_3$ $Na_{0.3}(AlMg)_2Si_4O_{10}(OH)_2.6H_2O$
EPAD450	SiO_2
EPAD550	SiO_2 $NaNO_3$
POCAD450	SiO_2 $Na_2S_2O_3$ MgS
POCAD550	SiO_2 $K_{1.2}Al_4Si_8O_{20}(OH)_4.4H_2O$
EPOCAD450	SiO_2 $Na_2S_2O_3$ $NaAl(SO_4)_2.11H_2O$ $Na_4Mn_5Si_{10}O_{24}(OH)_4.6H_2O$ $AlPO_4$
EPOCAD550	SiO_2

374

375 **3.2 Surface characterisation of the pelletised biochars**

376 **3.2.1 X-ray photoelectron spectroscopy**

377 XPS analysis was conducted on the exterior surfaces of POCAD450, POCAD550 and
378 EPOCAD450 pellets and the interior surfaces of a crushed pellet for POCAD450 and
379 EPOCAD450. A comparison of the C1s A, B, C and D; O1S A and B; and N1sA and B
380 bond states is depicted in Figure 1, and bonding mode designation is outlined in the
381 Supplementary Information.

382

Comparison of surface and whole sample XPS analyses of relative atomic % of bond states for POCAD450, POCAD550 and EPOCAD450

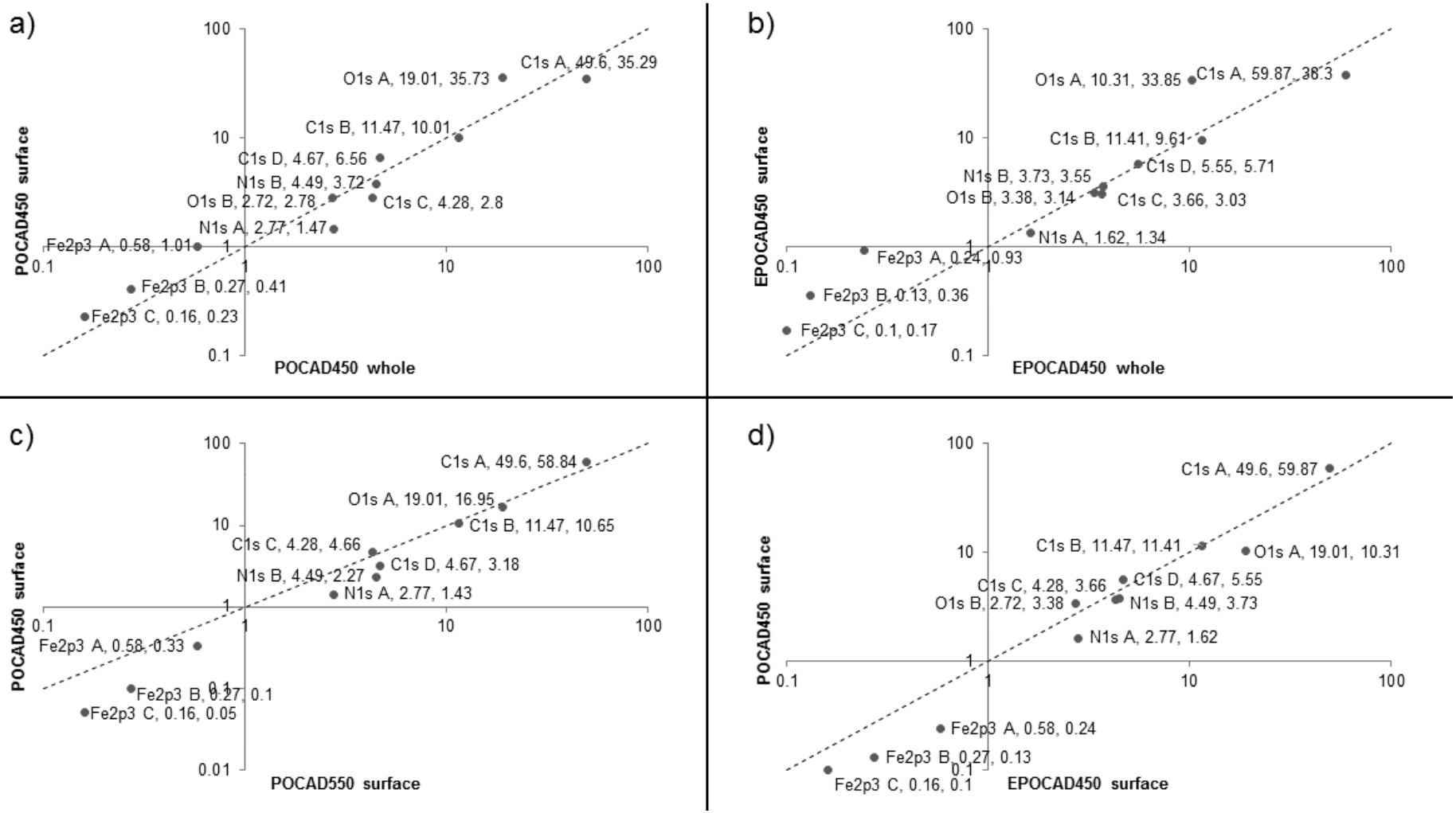

383

384 *Figure 1: Comparative log_{10}-log_{10} plots of relative atomic percentage of bond states*
385 *identified by XPS. a) Comparison of POCAD450 surface and whole sample analyses. b)*
386 *Comparison of EPOCAD450 surface and whole sample analyses. c) Comparison of*
387 *POCAD450 and POCAD550 surface analyses. Bond state O1s B was detected for*
388 *POCAD450 (relative atomic precentage 2.72 %) but not POCAD550, so this does not*
389 *appear on the plot d) Comparison of POCAD450 and EPOCAD450 surface analyses.*
390

391 The Fe2p3 results for POCAD450 and EPOCAD450 (Supplementary Table 3a) did not
392 support the presence of Fe(0) or predominantly Fe(II) state iron compounds, as these
393 were not detectable. The binding energy spectra indicate the possible presence of the
394 Fe(III) compound Fe_2O_3 or FeOOH on the surface of POCAD450 with a peak at 710.85
395 eV, whilst the Fe2p3 A peak observed at 711.51 eV in the interior surface indicates the
396 presence of either the Fe(II)/(III) compound Fe_3O_4 and/or surface Fe-O-PO_3^{2-}. This
397 suggests that the overall concentration of Fe_2O_3 or FeOOH is relatively small compared
398 with the concentration of Fe_3O_4 and/or surface Fe-O-PO_3^{2-}. The surface of the
399 EPOCAD450 also produced a Fe2p3 peak at 711.56 eV rather than 710.85 eV. The
400 shifting of the Fe2p3 A peak from 710.85 eV and associated Fe^{3+} satellite peak at
401 718.65 eV on the surface of POCAD450 to 711.56 eV and 720.33 eV respectively in
402 EPOCAD450 may indicate Fe-O-PO_3^{2-} bonding during P exposure, as phosphate-iron
403 interactions have been observed to cause similar energy shifts in previous studies
404 (Arshadi et al., 2015; Fang et al., 2015; Mallet et al., 2013). Both spectra indicate the
405 presence of iron sulfate compounds, which may be important.
406

407 The Fe2p3 peaks observed for the surface of POCAD550 differ slightly from those of
408 the 450°C pair. The Fe2p3 A peak, similar to the surface of EPOCAD450, is observed

409 at 711.52 eV, indicating either the presence of the Fe(II)/(III) compound Fe_3O_4 and/or
410 surface Fe-O-PO_3^2. The Fe2p3 B peak indicates the presence of $FeSO_4$, and/or is a
411 satellite of a Fe^{2+} peak. Importantly, the POCAD550 Fe2p3 C peak was uniquely
412 located at a lower energy of 708.82 eV, which indicates the presence of reduced Fe
413 compounds such as FeS_2, FeO and/or FeS.
414
415 Interpretation of the C, N, O and mineral peaks showed no differences in the proportion
416 of P, S, Ca, Fe and Na between POCAD450 and EPOCAD450 (Supplementary Table
417 3b). In terms of P, there is no difference in surface P concentration after P exposure as it
418 is very low relative to the native P concentration. The abundance of Si, C and N was
419 higher in relative terms for the EPOCAD450 pellet, while Al, O, F and Mg were
420 relatively less abundant. The only element present at a higher proportion on the surface
421 of EPOCAD450 compared to POCAD450 was C. In contrast to the whole sample
422 results, in the surface EPOCAD450 sample there was also lower detection of P, Si, Ca,
423 N, Fe, and Na compared to the surface of POCAD450.
424
425 Comparison of results for the surfaces of POCAD550 and POCAD450 pellets indicates
426 a higher proportion of C overall and lower proportions of P, S, N, O and Fe in
427 POCAD550. Heating of pure goethite (FeOOH) at temperatures > 600°C results in
428 sintering (Cornell and Schwertmann, 1996), so it is possible that the detection of a
429 lower proportion of Fe reflects sintering of Fe minerals at the 550°C HTT and a
430 decrease in overall Fe area, rather than loss of Fe from the biochar surface. The fact that
431 there was no difference in the distribution of the proportions of Al, Si, Ca and Mg
432 probably reflects the stability of minerals that contain these elements at higher
433 temperatures (Steenari and Lindqvist, 1998). At higher HTTs a higher proportion of C

434 relative to O may be expected, as O and H are more completely eliminated. It is possible
435 that proportionally more feedstock N, P and S was also eliminated in the preparation of
436 POCAD550 than POCAD450, on account of their own volatility (Magdziarz and Wilk,
437 2013).
438
439 **3.2.2 Laser ablation ICP-MS**
440 Mass spectral data from LA-ICP-MS analysis of POCAD450, POCAD550,
441 EPOCAD450 and EPOCAD550 were analysed to identify correlation of P with the
442 abundance of selected other elements: Al, Ca, Cu, Fe, K, Mg, Mn, Na, P, Pb, S and Si.
443 The selection of these elements was based on their predicted association with P and/or
444 their high concentrations within the biochars. The results are shown in Table 6, with
445 plots for the variation of elemental concentration per line scan in Supplementary
446 Figure 1. Phosphorus was significantly positively correlated with Mg, Al, K, Mn, Fe,
447 Cu and Pb for POCAD450, whilst after P exposure (EPOCAD450) the only strong
448 significant correlation ($\rho < 0.650$) was positive and was with Al. For POCAD550 there
449 was strong positive and significant correlation between P and Mg, Al, Si, K, Ca, Mn, Cu
450 and Pb. After P exposure (EPOCAD550), the correlations with Al, Si, K, Ca and Cu
451 remained highly significant. There was a marked difference between POCAD450 and
452 POCAD550 in the correlation coefficient of P with Fe (0.807 vs 0.462). For this reason,
453 correlations of Fe with other elements were also calculated (Table 6). Fe was strongly
454 and significantly positively correlated with P, Mg, S, Mn, Cu and Pb in POCAD450, but
455 only S and Mn in POCAD550. In EPOCAD550 the only significant correlation with Fe
456 that remained strong ($\rho < 0.650$) was with S, which was also positive.
457 *Table 6: Correlation coefficients of P and Fe to other elements analysed by LA-ICP-MS*
458 *($n = \sim 220$). Spearman's ρ is reported, except for correlations marked with ^{P}, where all*
459 *data were normally distributed so Pearson's product-moment correlation has been*

460 *reported. N.S. = no significant correlation.* * *= p<0.05,* ** *= p< 0.01,* *** *= p< 0.001,*

461 **** *= p< 0.001.*

462

463

	POCAD450		EPOCAD450		POCAD550		EPOCAD550	
	P	Fe	P	Fe	P	Fe	P	Fe
Na	0.330****	0.160*	0.385****	N.S.	0.432****	0.324****	0.433****	N.S.
Mg	0.767****	0.679****	0.572****	0.348****	0.651****	0.419****	0.629****	N.S.
Al	0.789****	0.618****	0.665****	0.333****	0.772****	0.396****	0.818****	N.S.
Si	0.521****	0.397****	0.515****	0.202**	0.669^{P,****}	0.453****	0.748****	N.S.
S	0.568****	0.866****	0.156*	0.342****	0.348^{P,****}	0.857****	N.S.	0.838****
K	0.737****	0.601****	0.586****	0.209**	0.671****	0.373****	0.866****	N.S.
Ca	0.520****	0.446****	0.517****	0.286****	0.772****	0.480****	0.850****	N.S.
Mn	0.747****	0.861****	0.585****	0.788****	0.696****	0.888****	0.515****	0.628****
Fe	0.807****	-	0.484****	-	0.462****	-	N.S.	-
Cu	0.713****	0.688****	0.402****	0.467****	0.742****	0.497****	0.737****	N.S.
Pb	0.765****	0.697****	N.S.	0.270****	0.714^{P,****}	0.530****	0.624****	N.S.

464 Principal Component Analysis (PCA) was also conducted on the LA-ICP-MS data to
465 identify the main clustering patterns of the elements on the surface of the biochars. The
466 PCA results are shown in Figure 2 and detailed information on the Principal
467 Components (PCs) of each sample is in Supplementary Tables S4–S7. Three PCs were
468 identified for POCAD450. The first PC axis separated sample locations from the line
469 scans (~220 for each biochar) enriched in Fe, Mn, S and Cu from sample locations
470 enriched in all other elements except for P, which was invariant along the second PC
471 axis. The concentration of all analysed elements increased along the second PC axis
472 apart from P. The clustering of elemental concentrations in the sample locations was
473 different after P exposure. Six PCs were identified for EPOCAD450. Along the first PC
474 axis, the concentrations of Al, Si, Ca, K, Na, Pb and S varied in the same direction,
475 whilst Mg, Cu, P, Mn and Fe concentrations varied together and separately from the
476 other group of elements. Again, the second PC axis separated sample locations which

contained either higher or lower concentrations of all of the analysed elements. Analysis of the POCAD550 data revealed five PCs and similar sample locations distribution to POCAD450 along the first PC, with a strong association between the concentrations of Fe and S, the variance of which was also related to that of Mn. All other elemental concentrations varied together, apart from Cu and Pb, which were invariant along the second PC axis. Similar to EPOCAD450, quite different elemental sample location distributions were identified after P exposure in EPOCAD550. Six PCs were identified, with sample locations enriched in Na, Mg and Al separated from sample locations enriched in Ca, Cu. Pb, Mn, Fe and S along the first PC axis. Iron and S were still strongly covariant, whilst K, P and Si were invariant along the second PC axis. Along the second PC axis, samples containing higher amounts of Fe and S separated from samples enriched in all other elements analysed. Unlike the transition observed in properties from POCAD450 to EPOCAD450, there was no evidence of dissociation of Fe and S in the higher temperature POCAD550 biochar after P exposure.

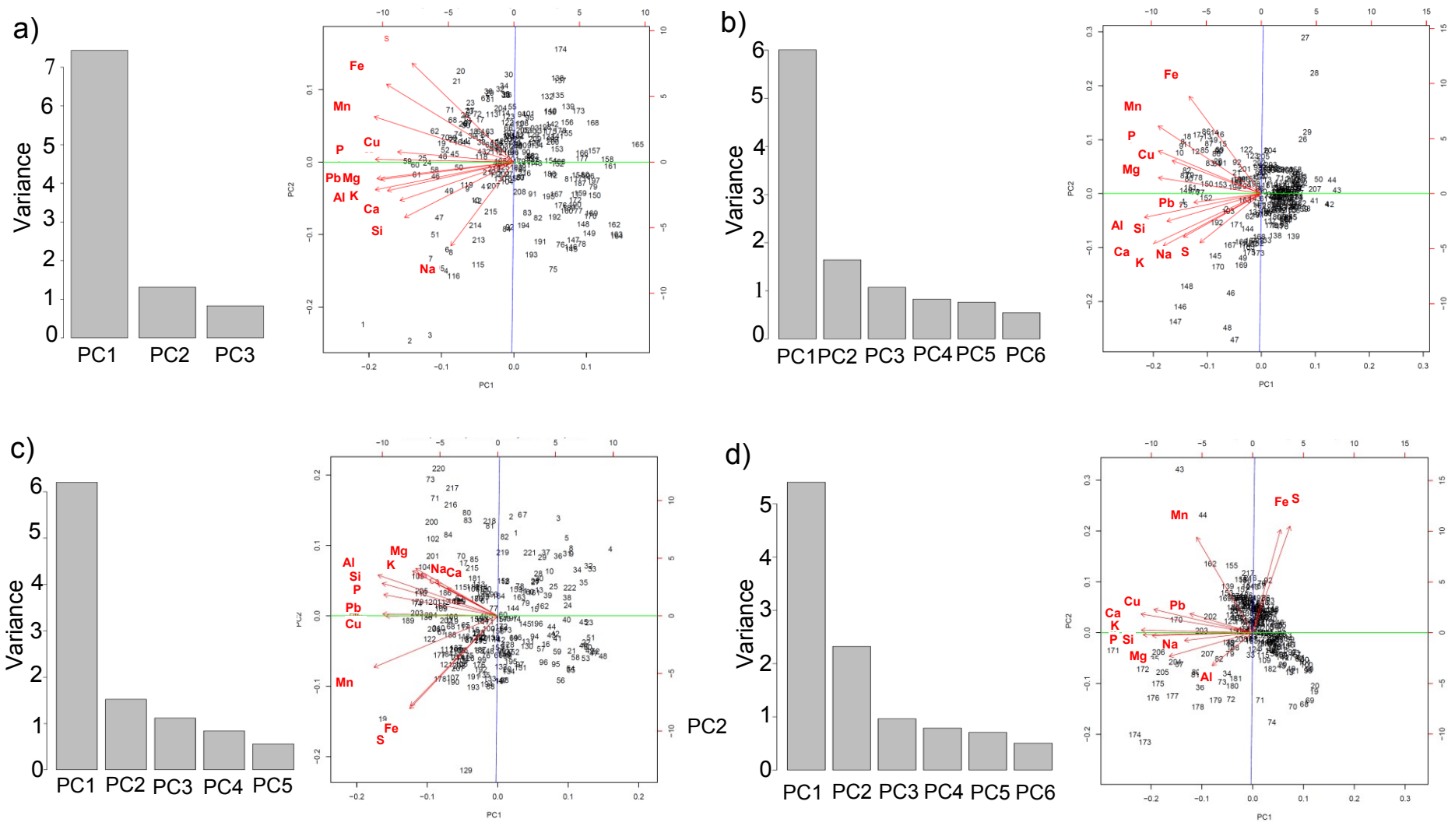
a)
Variance
PC1
PC2
PC3
Fe
Mn
P
Cu
Pb
Mg
Al
K
Ca
Si
Na
S
b)
Variance
PC1
PC2
PC3
PC4
PC5
PC6
Fe
Mn
P
Cu
Mg
Pb
Al
Si
Ca
Na
S
K
c)
Variance
PC1
PC2
PC3
PC4
PC5
Al
Si
P
Pb
Cu
Mg
K
Na
Ca
Mn
Fe
S
d)
Variance
PC1
PC2
PC3
PC4
PC5
PC6
Fe
S
Mn
Cu
Pb
Ca
K
P
Si
Na
Mg
Al

Figure 2: Principal component analysis of LA-ICP-MS spectral data obtained from a) POCAD450 b) EPOCAD450 c) POCAD550 and d) EPOCAD550. For each analysis n = ~220. The bar plots show proportion of variance of each principal component identified in the analysis. The adjacent plots how the distribution of samples along the first and second principal component axes, with arrows indicating the direction of the relevant vectors.

3.2.3 Scanning electron microscopy with energy dispersive X-ray spectroscopy

Visual comparison of SEM-EDX images from PAD450 and EPAD450 (Figure 3a-b) highlights the typical effect of P exposure on pores and mineral phases at the biochar exterior surface. Although the EDX spectra show similar element proportions overall, there is more P and Fe as well as considerably more exposed C (and somewhat less S) in EPAD (Figure 3c-d).

SEM highlighted surface heterogeneity at various scales in the pelletised biochars (Figure 4). Mineral phases in POCAD450 remain after P exposure (Figure 4a-1). Carbon surfaces are revealed (Figure 4a-2) and distinctive crystalline mineral phases are apparent (4a-3). The latter may have formed during the P exposure process or been exposed by dissolution of other phases. The masking of a carbon framework by a variety of Si-rich mineral phases is a feature commonly observed at high resolution (Figure 4c). Phosphorus deposits may be observed in positions also relatively enriched in Al, Ca and Fe (Figure 4f).

EDX mapping was used to visualise the co-location of elements in SEM images of EPOCAD450 in a spot identified as carbon framework with mineral deposits (and

representative of other sites with similar morphology) (Figure 5). The map shows clear separation of the carbon-rich area from other elements aside from O. The mineral deposits were shown to contain predominantly P, Si, Al and O. EDX mapping of a spot on POCAD550 (Figure 6) highlights the general elemental heterogeneity of the external surfaces of the biochars observed during the SEM analyses. The maps show the location of native P relative to other elements. Compared to EPOCAD550, a lower proportion of C was measured at the surface of POCAD550. The same was observed for EPOCAD450 compared to POCAD450. Aluminium, P, Fe and O were present across the whole spot of POCAD550 mapped in Figure 6, but were also concentrated in small 1–10 μm domains. Calcium was found to be located diffusely across the right side of the image, but only in concentrated domains to the left. Sulfur, Si and Mg were predominantly found in concentrated phases. The relative distribution of P, C, Ca, Si, Al and Fe can be seen in the overlay maps at the bottom of Figure 6, which supports the findings of Ca, Si and Al co-variation and Fe and P covariation in the LA-ICP-MS analysis of POCAD550 in Figure 2. Additional structural and chemical detail can be found in additional SEM images, EDX spectra and maps in Supplementary Figures S2-S6.

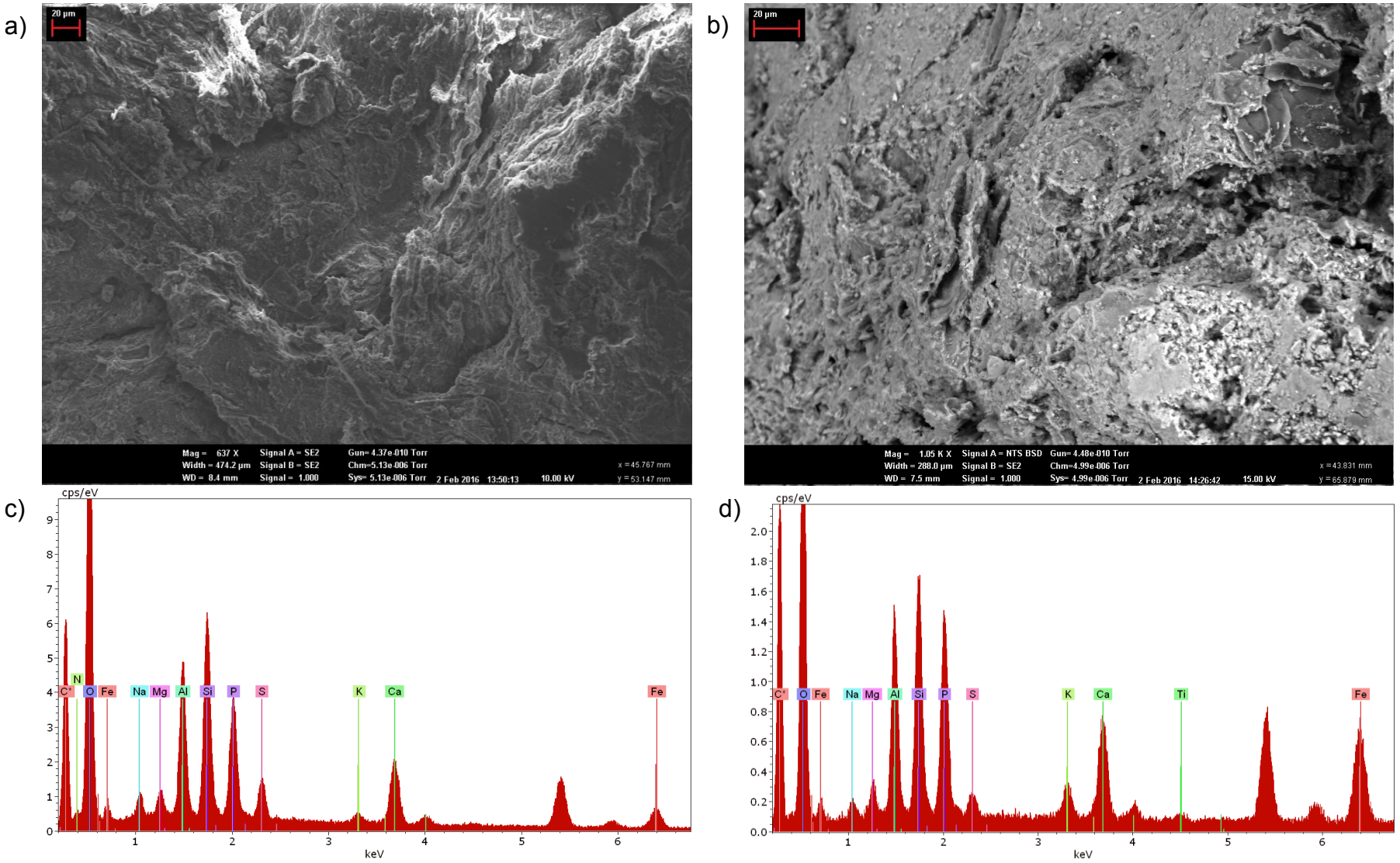

Figure 3: SEM and EDX spectrum of PAD450 (a,c) and EPAD450 (b,d) showing differences in surface morphology pre (PAD450) and post (EPAD450) P exposure.

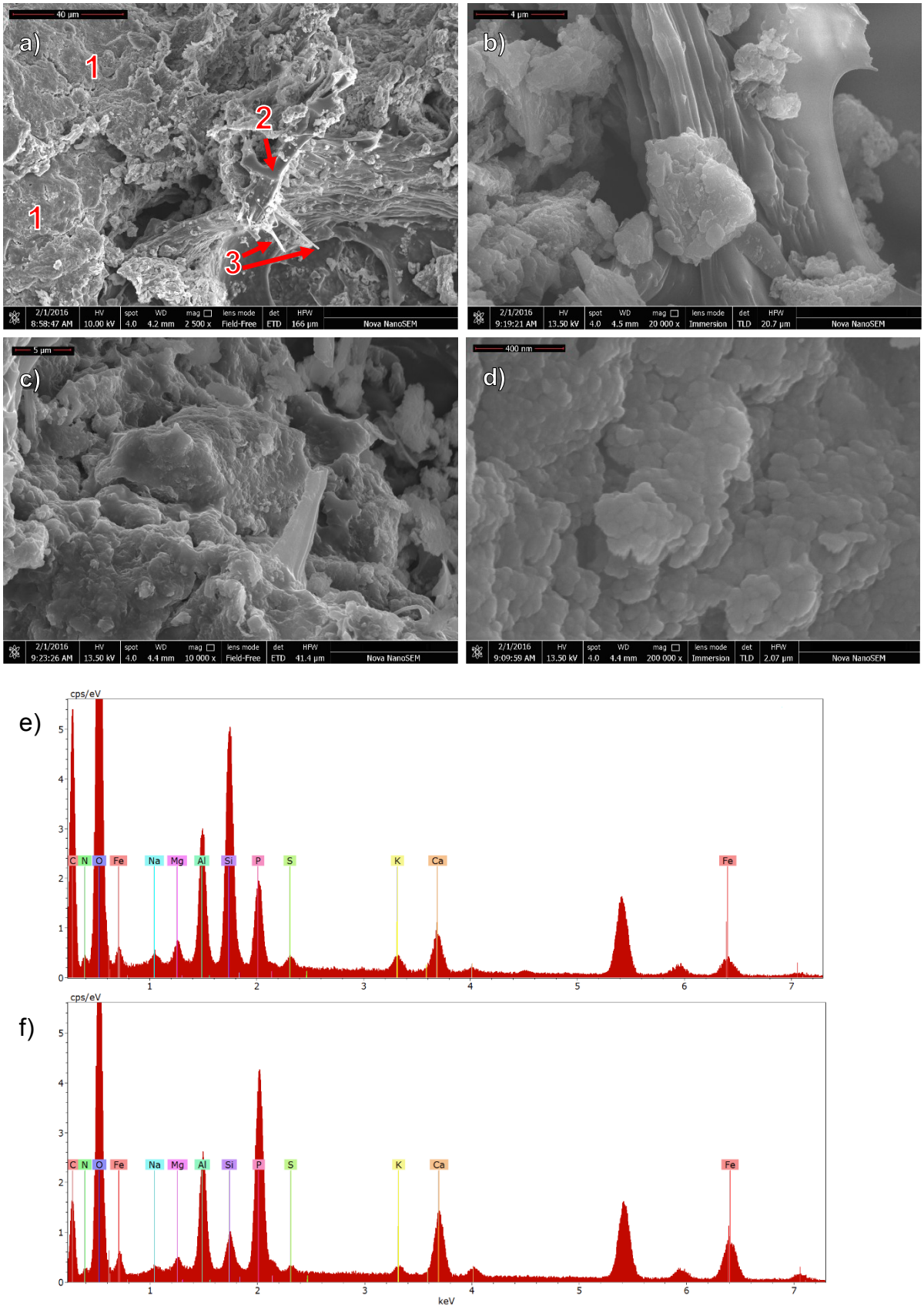

Figure 4: SEM-EDX data obtained from EPOCAD450. SEM image a) shows clay mineral phases (1), exposed carbon lattice (2) and newly formed or exposed mineral phases (3). SEM image b) shows mineral particles around the carbon lattice. Image c) shows the heterogeneous nature of the surface, and EDX spectrum d) shows the

elements present in c), e) shows high magnification SEM image and EDX spectra of P deposits on the surface of EPOCAD and f) shows the elements present in e).

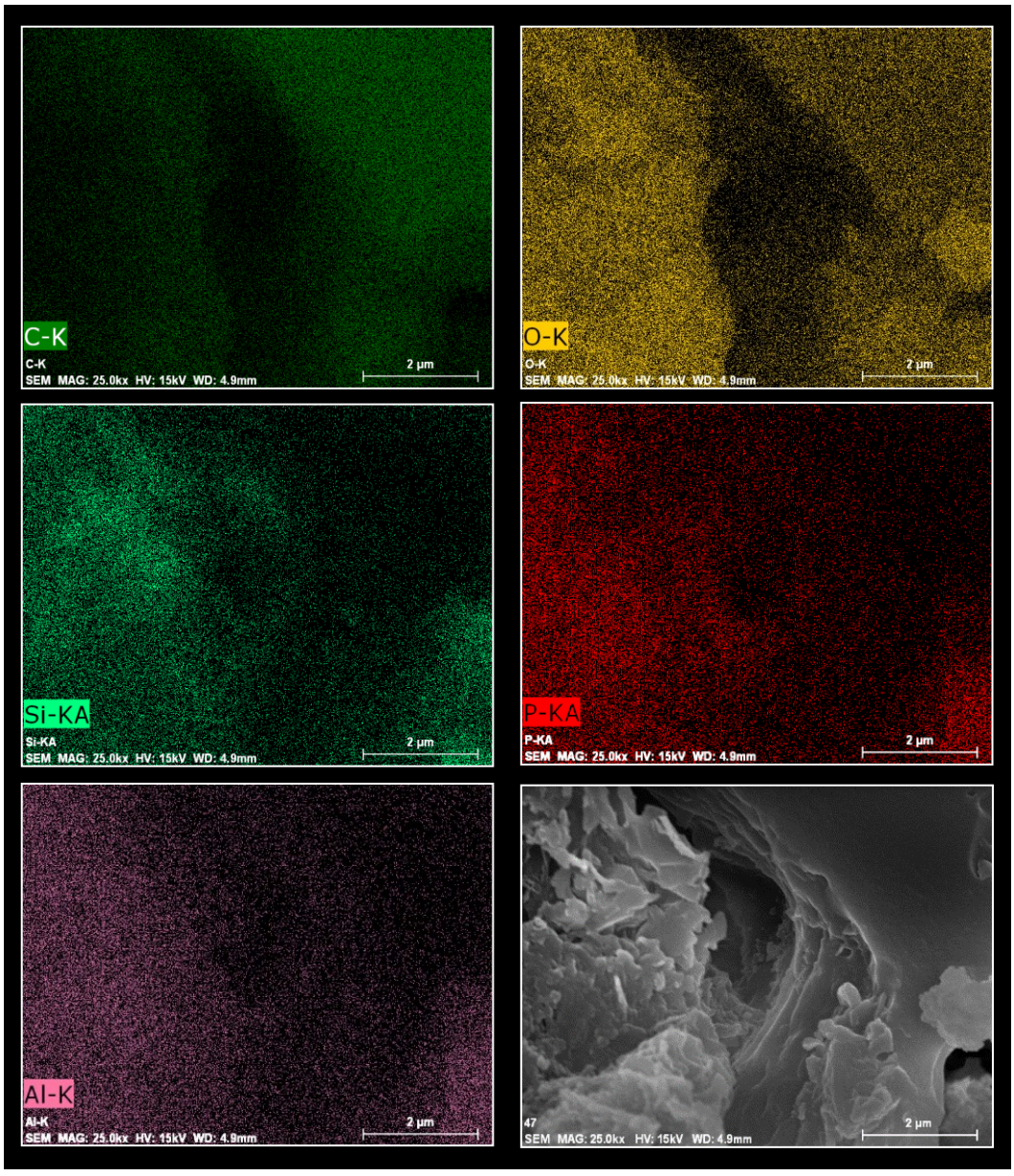

Figure 5: SEM-EDX map of EPOCAD450, showing spatial separation of C with O, Si, P and Al.

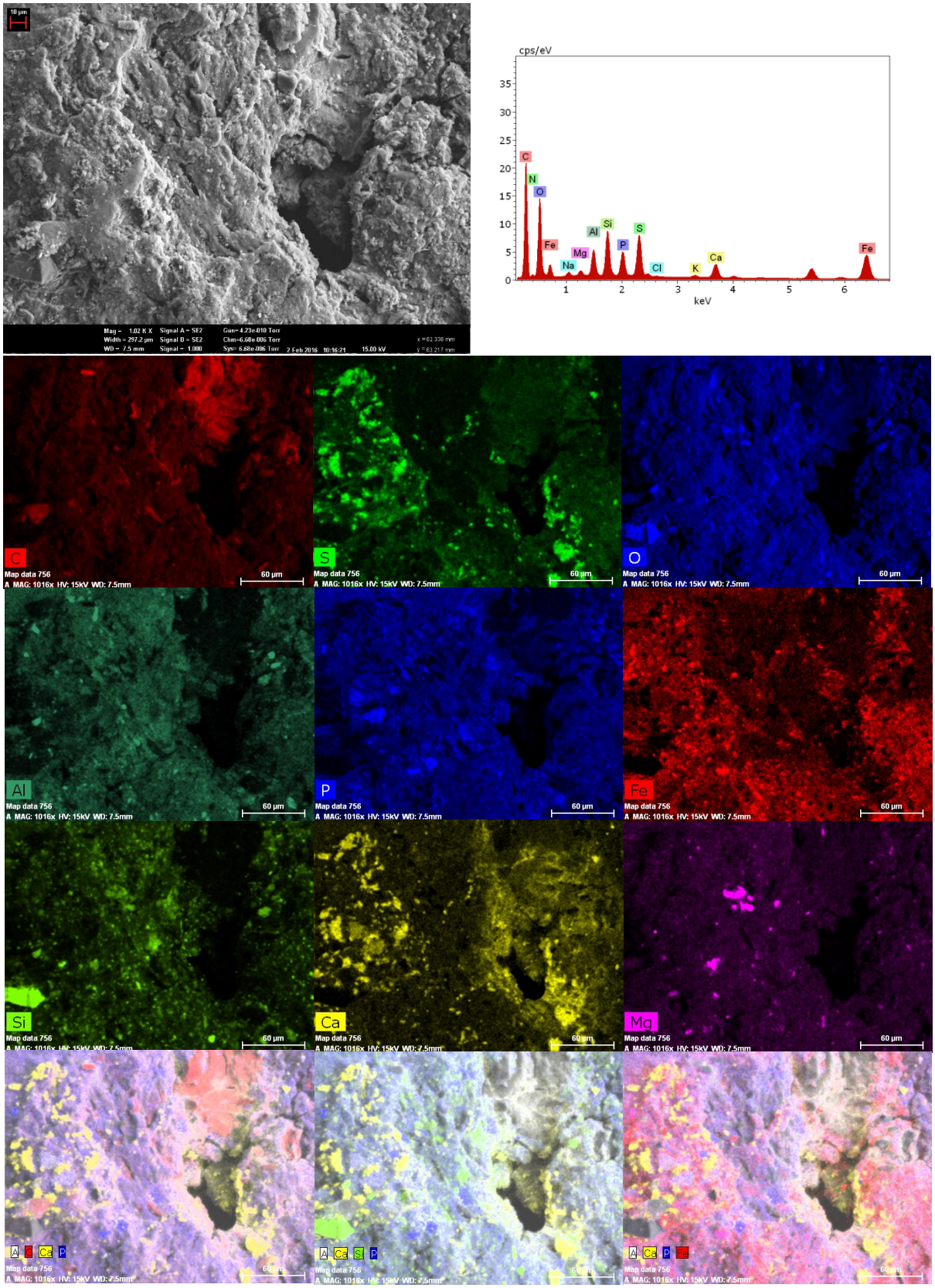

Figure 6: SEM-EDX map of POCAD550, showing the localisation of native P (centre), as well as C, S, O, Al, Fe, Si, Ca, and Mg. Overlay maps of C (red), Ca (yellow) and P (blue); Ca (yellow), Si (green) and P (blue); and Ca (yellow), P (blue) and Fe (red) are also shown.

617 **4. Discussion**

618 **4.1 Effect of feedstock composition, processing and pyrolysis conditions on P**

619 **capture**

620 The results of this study demonstrate that the interaction of P (as phosphate) with
621 sewage sludge-derived biochar is not a simple process which can be described by one
622 specific mechanism or element within the biochar matrix. At the macroscale (i.e. the
623 particle scale – mg and mm), each specific sewage sludge/ochre biochar material is
624 quite homogeneous, as demonstrated by the low standard deviations of replicated
625 determinations of total element composition by ICP-OES analyses of sample digests
626 (Tables 2 and 3) and of P uptake in the experiments with more uniform material sizes
627 (Shepherd et al., 2016). This reflects sufficient feedstock blending and indicates that the
628 pyrolysis process has occurred uniformly throughout the materials. In contrast, the
629 results of the XRD, SEM and LA-ICP-MS analyses highlight the microscale
630 heterogeneity of the materials. Although microscale heterogeneity is not necessarily
631 important for overall P capture capacity, more detailed studies of biochar microscale
632 structure in future work would provide better insights into mineralogy, which may
633 further assist in the selection of optimal HTT and feedstock blends for P capture and
634 release, especially when mineral wastes of variable composition are used as the source
635 of P-reactive elements.

636

637 **4.1.1 Iron plays a key role in P capture for biochars produced at 450°C**

638 Relatively small additions of ochre (10 % w/w) in the feedstock increased the Fe
639 concentration in pelletised POCAD biochars by 54–61% compared to the sewage
640 sludge-only equivalents (PAD). This is important, as Fe was the only element found to

641 be strongly and significantly correlated positively to P uptake after 5 days exposure to
642 P.
643
644 Considering the findings of Sibrell et al. (2009) examining P capture in ochres with
645 differing chemical compositions, it is possible that the superior P capture characteristics
646 demonstrated by AD450 could be related to the relatively equal content of Al and Fe in
647 AD450 compared to AD550 (1:1.12 vs 1:1.6). Although the ochre-containing biochars
648 captured more P from 5 days repeated exposure to a 20 mg l^{-1} solution, the mean P
649 capture by AD450 was slightly higher (though not significantly) than that of OCAD450
650 from both the 800 mg l^{-1} P (9.72 ± 0.657 mg P g^{-1} compared to 9.37 ± 0.872 mg P l^{-1})
651 and the 3 g l^{-1} P solutions (25.9 ± 5.10 mg P g^{-1} compared to 20.4 ± 6.35 mg P g^{-1}). This
652 indicates that, although a greater concentration of Fe may increase the rate of P capture
653 at low concentrations of external P solution, a balance of Al and Fe may favour the
654 reaction kinetics for P removal at higher external P concentration.(Ainsworth et al.,
655 1985) This is an important consideration for feedstock design, as mineral waste rich in
656 Al may be more suitable for combination with Fe-rich sewage sludge than iron ochre
657 for applications targeted at capturing P from high concentration P sources, but only if
658 they are to be used in non-acidic soils, or in conjunction with liming treatments to
659 mitigate Al toxicity to plants. Al was strongly and significantly correlated with P before
660 and after P exposure in the LA-ICP-MS analyses, further indicating the importance of
661 Al for P capture by biochar.
662

663 **4.1.2 Feedstock pelletisation affects elemental composition of biochar**

664 Comparison of the newly prepared pelletised biochars and non-pelletised biochars
665 previously described in Shepherd et al. (2016) showed that pelletisation and/or

continuous (rather than batch) pyrolysis processing results in greater overall retention of elements within the biochar matrix, relative to carbon. This is most likely due to a reduction in the loss of material to the gas phase, or a different trajectory of pyrolytic reactions in the continuous-flow furnace compared to the gradual heating process in a batch kiln. Rapid expulsion of gases from the pellets as the cold feedstock reaches the hot continuous-flow kiln may result in different pyrolytic reactions than if the feedstock was slowly heated to the same temperature, similar to the reported explanation for the differences between gas, oil and solid yield between fast and slow pyrolysis (Onay and Kockar, 2003).

4.1.3 Increasing highest treatment temperature changes iron oxidation state, sulfur interactions and mineral structure

Comparison of elemental variation in the first PC in the analysis of LA-ICP-MS results shows great similarity between POCAD450 and POCAD550, accounting for 77 and 61% of sample variance respectively. Covariance of Fe, S and Mn was identified in both, however the correlation of Fe and S was much stronger in POCAD550 than POCAD450 (Figure 2), indicating possible differences in mineral structure due to pyrolysis HTT.

The stronger relationship between Fe and S in POCAD550 compared to POCAD450 was supported by visual evidence from SEM-EDX. EDX analyses of POCAD450 revealed sites where Fe and S were covariant (as in Supplementary Figure S4a), and non-covariant (as in Supplementary Figures S4b-c and S5), whilst the same analysis of POCAD550 revealed more sites where Fe and S were found in higher concentrations together (Figure 6 and Supplementary Figure S7). These results may suggest reduced

691 iron species (Fe(I) or Fe(II)) are present in POCAD550, but not POCAD450 or
692 EPOCAD450, where Fe appears to be present in Fe(III) and mixed Fe(II/III)
693 compounds.
694
695 Considering these points together, is possible that at the 550°C HTT insoluble, reduced
696 Fe/S compounds have formed to a greater extent than at 450°C, in addition to complex
697 mixed mineral phases that contain both Fe and S. Further high-resolution analysis using
698 Thermogravimetric analysis–mass spectroscopy (TG-MS), soft X-rays and
699 Transmission electron microscopy (TEM) would be required to clarify this.
700
701 The ochre used in this study consisted of 100% goethite (Carr, 2012). When heated to
702 temperatures between 140–500°C in the presence of air, goethite transforms to
703 haematite by thermal dihydroxylation (Cornell and Schwertmann, 1996). Under
704 reducing pyrolysis conditions and the presence of carbon, it is also possible that
705 magnetite (Fe_3O_4, Fe (II)(III) oxide) and maghemite (γFe_2O_3, Fe(III) oxide) forms
706 (Campbell et al., 1997). Thermal treatment of goethite results in the development of
707 microporosity due to expulsion of water from the mineral lattice, creating more surfaces
708 with which P can react. Pore sizes increase further as temperatures increase, however, as
709 previously discussed, above 600°C the mineral sinters, which results in a large decrease
710 in porosity (Cornell and Schwertmann, 1996). Hence pyrolysis HTTs of less than 600°C
711 may be necessary for biochars containing large amounts of iron oxyhydroxides if high
712 surface area and P reactivity are desired.
713
714 **4.2 P capture processes**
715 **4.2.1 The role of organic functional groups on biochar surfaces in P capture**

716 Despite the modest pyrolysis temperatures used in this study, SEM-EDX mapping and
717 XPS analysis did not provide strong evidence for C-O-P bonding, or carbon
718 functionality generally. It has been suggested that phosphate could undergo ligand
719 exchange with hydroxyl or carboxyl groups on the surface of the biochar carbon lattice
720 (Laird and Rogovska, 2015), however ligand exchange reactions only occur in metal
721 complexes. Synthesis of the proposed phosphoester species proceeds via a condensation
722 reaction, is favoured by decreasing pH (inconsistent with biochar surfaces), and requires
723 high temperatures, condensing agents or condensed phosphate reagents, which also
724 require significant temperatures for synthesis (Gull et al., 2014). In biological systems
725 (at pH values closer to 7) the phosphorylation reaction requires enzyme catalysis, so the
726 proposed mechanisms are unlikely to occur on biochar surfaces in environmental
727 systems unless mediated by an organism which has some biological need to perform
728 this reaction.
729
730 There is no evidence, in this study or in the literature, to suggest that the carbon fraction
731 of biochar plays a major role in P capture, other than providing an essential support on
732 which the mineral elements which do interact with P can be anchored, and improving
733 the value of the end-product for use in agriculture. A significant increase in P sorption
734 was observed in washed compared to unwashed oak biochar (Hollister et al., 2013),
735 however the concentration of P sorbed by even the washed biochar was quite small
736 (0.077 mg P g^{-1}, 13.5% of the lowest amount of P captured in this study), so the effect
737 of washing to expose carbon surfaces appears to be over-estimated. The increasingly
738 common practice of adding chemical elements to biochar for P capture enhancement is
739 additional evidence for this assertion (Chen et al., 2011; Fang et al., 2015; Li et al.,
740 2016; Park et al., 2015; Ren et al., 2015; Yao et al., 2011; Zhang et al., 2013, 2012). It is

741 evident that metal cation-mediated interactions with organic functional groups on
742 biochar surfaces (or precipitation reactions) explain the high P capture capacities
743 demonstrated by particular biochars.
744
745 The point of zero charge (PZC) of biochars reported in the literature are generally low
746 (Mukherjee et al., 2011; Qiu et al., 2009; Silber et al., 2010), so it is likely that at pH > 3
747 biochar surfaces will be negatively charged. Theoretically, at high pH a hydroxyl or
748 carboxyl group on the surface of biochar will be deprotonated in solution, forming an
749 oxyanion which will be resonance stabilised by the delocalisation of electrons in the
750 aromatic biochar structure. This makes these groups more acidic than the equivalent
751 group in an aryl alcohol. The oxyanion will be nucleophilic, and could attack the
752 phosphate P (capturing the phosphate from solution), which, under basic conditions,
753 will be relatively electron poor due to the presence of two electronegative oxyanions
754 and a C=O group. The likelihood of these two negatively charged species coming
755 together for reaction is low, however, due to electrostatic repulsion. Cations in solution
756 may reduce this effect but, even so, the nucleophilic attack of the phosphate P by the
757 biochar oxyanion is also sterically hindered. The equivalent argument can be made for
758 the potential interactions between phosphate and N-heterocycles on biochar surfaces.
759 Whilst not chemically impossible, the likelihood is low of these reactions contributing
760 in any significant way to P capture mechanisms in biochar materials in wastewater
761 treatment systems.
762

763 **4.3 Conceptual model of P capture by biochar from aqueous solution**

764 **4.3.1 Initial solubilisation and mobilisation of native biochar components**

765 In the P capture experiments biochar is held in aqueous P solution buffered at pH 7. A
766 simplified reaction mechanism for the interaction of aqueous phosphate with metal
767 oxides on the biochar surface is given in Figure 7. Soluble organic and mineral
768 compounds are presumably released into solution at a rate that depends on their
769 proximity to the surface of the biochar (limited by pore size and connectivity) as well as
770 their solubility in the P solution and binding mechanisms. As demonstrated for soil, the
771 energy required for P exchange from soil water to soil particles is very similar to that of
772 the reverse reaction (Barrow, 2015), so the direction of this reaction in biochar (i.e. P
773 capture or release) will be similarly dictated partly by the amount of P already within
774 the biochar structure relative to its capacity for P uptake (probably related to the
775 concentration and composition of certain mineral components).

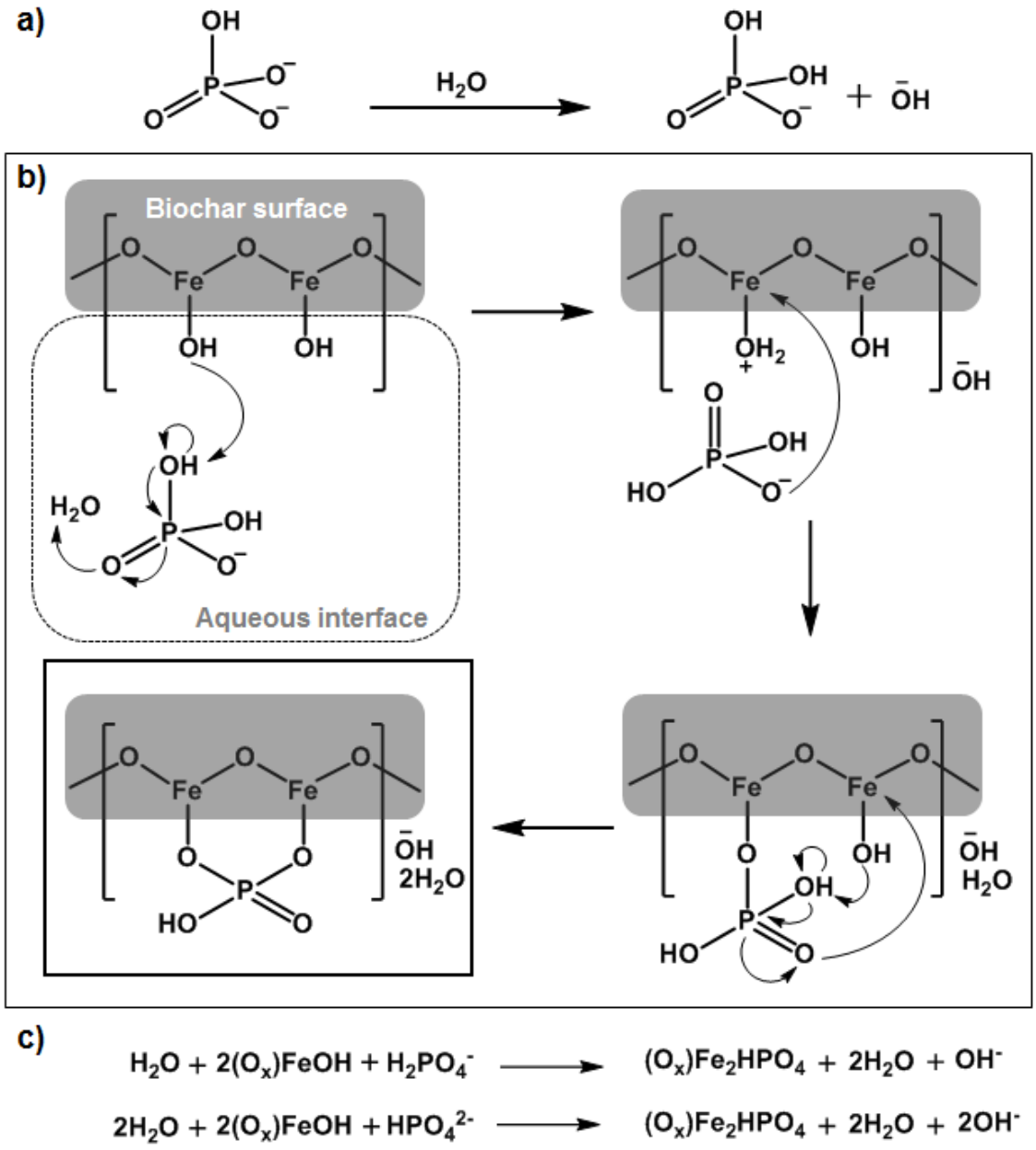

Figure 7: Likely predominant AD sewage sludge biochar P sorption mechanism where the metal = $M^{2+/3+}$. Iron oxyhydroxides are presented based on the experimental evidence pointing to their significance in these biochars. (a) In a pH 7 buffered aqueous environment the basic phosphate species HPO_4^{2-} reacts with water to form the acidic $H_2PO_4^-$ species. (b) Deprotonation of a phosphate hydroxide moiety by the iron oxyhydroxide, followed by phosphate rearrangement and subsequent deprotonation of a water molecule, producing hydroxide, regenerates $H_2PO_4^-$ and renders the iron prone to nucleophilic attack by phosphate. The process can repeat on an adjacent

785 *ironoxyhydroxide moiety, forming a stabilised ring structure. (c) Balanced equations*
786 *for the overall reaction where either $H_2PO_4^-$ or HPO_4^{2-} is the starting species.*
787
788 The initial process of solubilisation of different phases within the biochar structure is
789 likely to open up the pore structure, as evident in Figures 2–4 and Supplementary
790 Figures S2–S6. It is possible that, due to the comparatively low ratio of C compared to
791 minerals in the sewage sludge feedstock, the carbon structure will contain a range of
792 pore sizes. Physical determinations of porosity were not undertaken in this study, but
793 visual SEM observation supports this hypothesis. During pyrolysis non-volatile mineral
794 elements are likely to restrict the formation of aromatic sheets and promote pore
795 formation (Rawal et al., 2016).
796
797 XPS analysis of surface and whole samples of POCAD450 and EPOCAD450 revealed a
798 "loss" of P, Si, Ca, N, Fe, and Na from the exterior (but not interior) surfaces after P
799 exposure. It is possible that this reflects solubilisation and loss of these elements from
800 the surface into solution during P exposure, but another explanation is that the elements
801 were re-arranged on the surface after initial solubilisation, forming localised mineral
802 complexes (Figures 8 and 9). The formation of these complexes would result in
803 exposure of the carbon lattice, as seen in the SEM images (Figures 2–4), coupled with
804 mineral expansion out from (rather than laterally across) exterior surfaces. In XPS
805 analysis after P exposure mineral elements located closer to the biochar surface might
806 not be detected owing to masking by mineral layers and thus falsely appear to been
807 "lost". The LA-ICP-MS results also indicate that solubilisation and re-association
808 occurred, with the number of significant correlations between P and other elements
809 lower in EPOCAD than corresponding POCAD biochars.

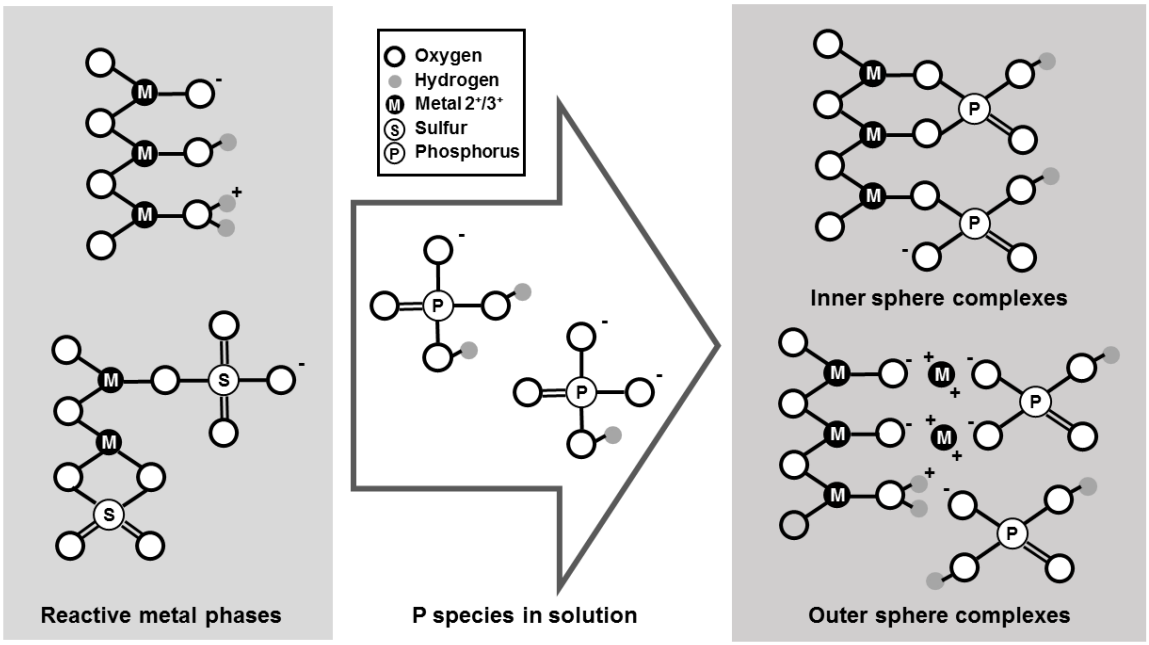

Figure 8: Phosphate-reactive metal phases on the biochar surfaces in these biochars. The degree of hydrogenation of the metal oxides decreases with increasing pH and is affected by the pyrolysis highest treatment temperature (HTT). Experimental observations indicate that in addition to hydroxyl ligand exchange, biochar phosphate capture also occurs at sites vacated by sulfate. These reactive sites can form inner sphere and outer sphere compounds with phosphate, with some examples shown.

The SEM-EDX, LA-ICP-MS and XRD analyses collectively suggest that non-soluble mineral phases remain on and in the biochar structure after P exposure. If this is correct, non-soluble phases anchored on biochar surfaces via soluble organic or mineral phases would become detached from the surface over time, as other phases dissolve. Minerals on the external surface of the biochar would then be lost from biochar into solution, those remaining in pores either being washed out over time or remaining trapped. Surface area to volume ratio and pore structure may affect the release of less soluble mineral phases.

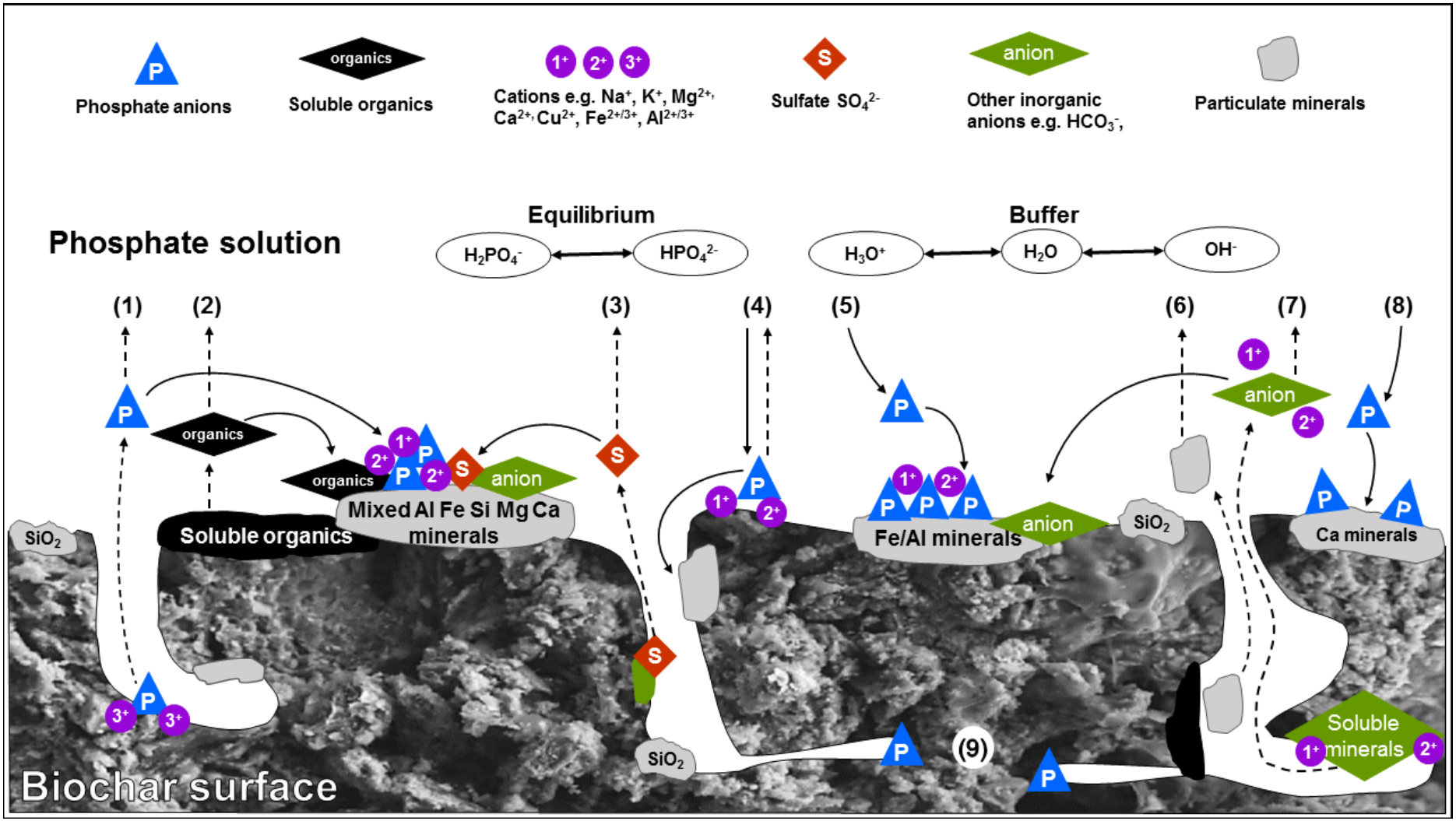
Phosphate anions
organics
Soluble organics
Cations e.g. Na+, K+, Mg2+, Ca2+, Cu2+, Fe2+/3+, Al2+/3+
S
Sulfate SO4 2-
anion
Other inorganic anions e.g. HCO3-,
Particulate minerals
Phosphate solution
Equilibrium
H2PO4-
HPO4 2-
Buffer
H3O+
H2O
OH-
(1)
(2)
(3)
(4)
(5)
(6)
(7)
(8)
(9)
Soluble organics
Mixed Al Fe Si Mg Ca minerals
Fe/Al minerals
Ca minerals
Soluble minerals
SiO2
Biochar surface

826

Figure 9: Graphical representation of reactions which occur when biochar is placed in a pH 7 buffered phosphate solution. (1) Dissolution of phosphate from soluble ash/mineral phases. Phosphate may be released into solution or re-associate with biochar surfaces via mineral or organomineral interactions with other mixed species, such as Al, Fe, Si, Mg, Ca, K and Na in these materials. (2) Dissolution of soluble organic species from surfaces. These species may stay in solution or re-associate with species on the surfaces in organomineral clusters. (3) Dissolution of sulfate minerals (as observed in the biochars produced at 450°C). Sulfate may stay in solution or re-associate with surfaces in mineral or organomineral clusters. (4) Electrostatic association of phosphate to biochar surfaces via cation mediated interactions with surface organic functional groups. Phosphate may either be re-released into solution due to the relative weakness of the interactions or react chemically with mineral phases resulting in stronger retention. (5) Chemisorption of phosphate to iron and/or aluminium oxide phases on the biochar surfaces. (6) Release of insoluble ash and mineral phases into the aqueous phase due to weak binding or lack of binding to biochar surfaces. (7) Solubilisation of other minerals from within the biochar structure. (8) Precipitation of phosphates from solution with calcium mineral phases. (9) Native phosphate phases will be found within the biochar pore structure and will not be immediately accessible for dissolution, as per scenario (1). These phases will be released more gradually, over time.

4.3.2 Interaction of P with biochar surfaces and mobilised elements

In a solution phosphate interacts with solubilised mineral elements to form phosphate complexes which, depending on the phosphate coordination mechanism, can also interact with soluble organic compounds or organic surface-bound functional groups.

852 Once chemically bound or precipitated onto a surface phosphate-mineral and -
853 organomineral compounds can interact with other elements in solution. Phosphate
854 ligands can be labile and coordinate to metals in different ways, e.g. monodentate vs
855 bidentate coordination via O atoms (Arai and Sparks, 2001). Thus the way in which
856 phosphate binds to the surface of biochar is dependent on the other species present and
857 will change over time as different compounds dissolve and the local environment
858 changes (see Figures 8 and 9).
859

860 **4.3.2.1 Monovalent cations interrupt P capture and enhances P release**

861 For the 20 mg l^{-1} P treatments (Shepherd et al., 2016), Al, Cu, K, Na, and Zn
862 concentrations in the biochars were all significantly negatively correlated with P capture
863 on day 1. In addition, Pb was negatively correlated with P capture on day 5 (Table 4).
864 The presence of high concentrations of mono- and divalent salts in the biochar samples
865 that could dissolve in the P exposure experiments (Tables 2 and 3) may result in
866 stabilisation of the $H_2PO_4^-$ anion in solution, reducing the rate of capture. Furthermore,
867 K from the K_2HPO_4 used to make the phosphate solution would exacerbate this effect.
868 Indeed the lack of similar correlations in the day 5 and 800 mg P l^{-1} treatments supports
869 this interpretation, as by day 5 much of the K and Na will have leached from the biochar
870 and, in the higher concentration experiments the concentration of phosphate will be
871 much higher relative to the concentrations of K and Na leaching from the biochar.
872 Positive correlation of Na with P release also supports this interpretation.
873

874 In the 800 mg l^{-1} P experiments and not the 20 mg l^{-1} P experiments, however, K is
875 negatively (but not significantly) associated with P release (Pearson's product-moment
876 correlation = -0.636, p value = 0.175). This may be an electrostatic effect, where excess

877 K from the higher concentration treatment (added with the phosphate solution as
878 K_2HPO_4) interacts with the biochar surface making it more positively charged, reducing
879 the repulsion effect that slows down P capture over time (Barrow, 2015). As ash is
880 washed from the biochar during the experiment, more of the negative carbon functional
881 groups of the biochar are exposed, increasing the possibility for K to interact in this
882 way. For the higher concentration treatments at least, any effect of K on P capture and
883 release is most likely an artefact of the experimental setup and may not be observed
884 when the materials are used in a wastewater treatment plant.
885
886 **4.3.2.2 Mixed Fe and Al minerals are involved in P capture**
887 Biochar Fe concentration was significantly positively correlated with P capture and
888 negatively correlated with P release. As well as P captured during the adsorption
889 experiments, XPS analysis indicated that native P is associated with Fe in the biochars.
890 Phosphorus and Fe can react during pyrolysis, especially when ochre is present in the
891 feedstock as during pyrolysis as it can act as an acid catalyst (Joseph et al., 2013). Clay,
892 when heated, can liberate a range of chemical species including HF, HC1, HBr, H_2S and
893 HP (Heller-Kallai et al., 1988). Interior biochar surfaces characterised by XPS showed
894 the presence of Fe_3O_4 in both POCAD450 and EPOCAD450 as well as the surface of
895 the latter, whilst Fe_2O_3 was only identified on the surface of POCAD450. It is possible
896 that P exposure acts to prevent oxidation of the biochar surfaces, and that P sorption
897 occurs without oxidising Fe(II), therefore possibly only occurring at Fe(III) sites, but
898 additional XPS analysis would be required to fully explore these hypotheses.
899

900 For pelletised biochar from sludge–ochre mixes correlation analysis using LA-ICP-MS
901 data showed strongly significant positive correlation between the concentration of P and

902 Al after P exposure (EPOCAD450) or with Al, Si, K, Ca and Cu (EPOCAD550). PCA
903 of LA-ICP-MS data for the P-exposed EPOCAD450 biochar showed that P
904 concentration variation was related to that of Fe, Mn, Cu and Mg in the first and second
905 PCs. Compared to POCAD450, the relationship between the variance of Fe and Mn
906 with P was stronger whilst the relationship of P with the variance of S decreased,
907 suggesting replacement of sulfate by phosphate as a potential sorption mechanism,
908 which is supported by the SEM-EDX data. This was not the case for EPOCAD550, in
909 which P concentration variation was not related to that of Fe, S and Mn in the first and
910 second PCs, yet the relationship between the variance of Fe and S in POCAD550 was
911 maintained after P exposure, suggesting a different mechanism of P capture compared
912 to POCAD450. The bulk P capture for POCAD450 and POCAD550 were nearly
913 identical (0.95 ± 0.18 mg P g^{-1} and 0.95 ± 0.23 mg P g^{-1}, respectively), so although it
914 appears that different mechanisms predominate in biochars prepared at contrasting
915 HTTs, the net effect on P capture is similar. The heterogeneity of the biochars and
916 therefore P capture mechanisms most likely increases, as evidenced by the increased
917 number of PCs in the EPOCAD compared to POCAD biochars, as well as the smaller
918 relative contribution of PC1 in the former cases. These analyses provide information on
919 the main sources of variation between sample locations on the biochar surface but also
920 highlight the high amount of heterogeneity on the microscale.
921

922 Although Ca was only identified as strongly significantly correlated to P capture in the
923 LA-ICP-MS analysis of EPOCAD550, as it is present at a relatively high abundance in
924 the biochars it is likely that precipitation of P by Ca occurs in each of them to some
925 extent. The buffered pH 7 of the system may not favour this reaction, which could
926 explain why Ca concentration did not correlate with P capture consistently. High P

927 capture from mallee tree biochar produced at 720°C HTT has been reported in the
928 literature (Zhang et al., 2016). The authors suggest that the mechanism of P capture is
929 via precipitation of P as $CaHPO_4$ by substituting for HCO_3^{2+} and OH^- on $CaHCO_3^+$ or
930 $Ca(OH)_2$ mineral surfaces of the biochar. This seems quite likely, as the biochar had a
931 pH of 10.2, which strongly favours Ca phosphate precipitation, and contained 1.3% Ca
932 by weight but no Fe or Al. Importantly, whilst washing of the biochar with deionised
933 water significantly increased P capture but did not greatly affect Ca concentration,
934 washing with acid significantly decreased P capture, with an associated decrease of Ca
935 content in the biochar to 0.1%. The precipitation of hydroxyapatite was observed in
936 similar experiments obtained using cement-bound ochre to capture P from a non-
937 buffered P solution (Littler et al., 2013).
938
939 **4.4 Practical significance**
940 Considered together, our results suggest that the mechanisms of P retention by biochar
941 made from sewage sludge, although homogeneous and reproducible at the macroscale,
942 will be highly heterogeneous at the micro and nanoscale and dependent on: (1)
943 feedstock composition, in particular Fe and Al concentration (but also Ca and Mg); (2)
944 pyrolysis conditions, where these affect the solubility of the mineral elements formed
945 during the process; (3) the reactivity of the chemical elements released from the soluble
946 mineral elements into solution during the P sorption/capture process; (4) the pH of the
947 system, as this directly affects (3); and (5) the concentration of phosphate in solution as
948 this will shift the equilibrium of the reaction, which has a similar activation energy in
949 the forwards and backwards directions (Barrow, 2015).
950

This study has shown that pelletisation of sewage sludge leads to retention of elements within the biochar structure and/or contamination from the pelletising process compared to non-pelletised sewage sludge. This is a positive feature for retention of nutrients, but could lead to retention of potentially toxic elements (PTEs) inhibiting the environmental suitability of biochar.

Our results also highlight the importance of minerals within the biochar structure for their observed functionality in soil. When added to soil to improve soil quality in some way, biochar mineral composition should be considered in combination with the nutrient status of the biochar and the soil, as well as pH, in order to predict the effect on nutrient mobility in the system. The PZC of the different minerals is an important aspect, as this will dictate whether the mineral surfaces will be positively or negatively charged at the native pH of the biochar, controlling the interactions between these phases in biochar and nutrients or PTEs. The pH of the environment into which biochar is added will also have an effect on this, so it is important to consider when tailoring a biochar material to a specific purpose.

5. Conclusions

Sustainably produced biochar prepared from pelletised digested sewage sludge has an affinity for P in solution higher than activated carbon and thus potential for P capture and recycling. The inclusion of goethite-containing ochre as a minor ingredient prior to sludge prior to pelletising and pyrolysis results in biochar that captures more P than pelletised biochar from sludge only. Based on correlation analysis and surface examination, Fe and Al present in complex mineral phases containing also Si, Mg and Ca explained the P capture properties. Pyrolysis yields a greater proportion of less

soluble Fe/S minerals at 550°C than at 450°C, which may result in lower P capture over the long term.

Acknowledgements

The authors thank Ben Pace, and Ms. Rabeya Akter (MSc-BSc-hons, Chemistry) at UNSW for their assistance with analyses, Dr Ondřej Mašek at the University of Edinburgh for access to UKBRC pyrolysis facilities and Dr Wolfram Buss for production of biochar. Dr Annie Colebatch and Dr Roy Doyle gave generously of their time for discussions of chemical mechanisms. Jessica Shepherd's PhD is supported by the University of Edinburgh Principal's Career Development Scholarship and Edinburgh Global Research Scholarship, and ICON Canberra, Australia.

References

Ainsworth, C.C., Sumner, M.E., Hurst, V.E., 1985. Effect of Aluminum Substitution in Goethite on Phosphorus Adsorption: I. Adsorption and Isotopic Exchange. Soil Sci. Soc. Am. J. 49, 1142–1149. doi:10.2136/sssaj1985.03615995004900050015x

Angst, T.E., Sohi, S.P., 2013. Establishing release dynamics for plant nutrients from biochar. GCB Bioenergy 5, 221–226. doi:10.1111/gcbb.12023

Arai, Y., Sparks, D.L., 2001. ATR–FTIR Spectroscopic Investigation on Phosphate Adsorption Mechanisms at the Ferrihydrite–Water Interface. J. Colloid Interface Sci. 241, 317–326. doi:10.1006/jcis.2001.7773

Arshadi, M., Zandi, H., Akbari, J., Shameli, A., 2015. Ferrocene functionalized nanoscale mixed-oxides as a potent phosphate adsorbent from the synthetic and real (Persian Gulf) waters. J. Colloid Interface Sci. 450, 424–433. doi:10.1016/j.jcis.2015.03.026

1001 Barrow, N.J., 2015. Soil phosphate chemistry and the P-sparing effect of previous
1002 phosphate applications. Plant Soil 397, 401–409. doi:10.1007/s11104-015-2514-5
1003 Barrow, N.J., 1983. A mechanistic model for describing the sorption and desorption of
1004 phosphate by soil. Eur. J. Soil Sci. 66, 9–18. doi:10.1111/ejss.12198
1005 Bhatnagar, A., Sillanpää, M., 2011. A review of emerging adsorbents for nitrate
1006 removal from water. Chem. Eng. J. doi:10.1016/j.cej.2011.01.103
1007 Buss, W., Graham, M., Shepherd, J.G., Masek, O., 2016a. Suitability of marginal
1008 biomass-derived biochars for soil amendment. Sci. Total Environ. 547, 314–322.
1009 doi:10.1016/j.scitotenv.2015.11.148
1010 Buss, W., Graham, M.C., Shepherd, J.G., Mašek, O., 2016b. Suitability of marginal
1011 biomass-derived biochars for soil amendment. Sci. Total Environ. 547, 314–322.
1012 doi:10.1016/j.scitotenv.2015.11.148
1013 Campbell, A., Schwertmann, U., Campbell, P., 1997. Formation of cubic phases on
1014 heating ferrihydrite. Clay Miner. 32, 615–622. doi:10.1180/claymin.1997.032.4.11
1015 Carr, S., 2012. An Investigation into Phosphorus Removal by Iron Ochre for the
1016 Potential Treatment of Aquatic Phosphorus Pollution. The University of
1017 Edinburgh.
1018 Chen, B., Chen, Z., Lv, S., 2011. A novel magnetic biochar efficiently sorbs organic
1019 pollutants and phosphate. Bioresour. Technol. 102, 716–723.
1020 doi:10.1016/j.biortech.2010.08.067
1021 Cornell, R.M., Schwertmann, U., 1996. The iron oxides: Structure, properties, reactions,
1022 occurrence and uses, 1st ed. VCH, Weinheim.
1023 Cucarella, V., Zaleski, T., Mazurek, R., Renman, G., 2008. Effect of reactive substrates
1024 used for the removal of phosphorus from wastewater on the fertility of acid soils.
1025 Bioresour. Technol. 99, 4308–4314. doi:10.1016/j.biortech.2007.08.037

1026 Dobbie, K.E., Heal, K. V., Aumônier, J., Smith, K. a., Johnston, a., Younger, P.L.,
1027 2009. Evaluation of iron ochre from mine drainage treatment for removal of
1028 phosphorus from wastewater. Chemosphere 75, 795–800.
1029 doi:10.1016/j.chemosphere.2008.12.049
1030 Downie, A., Crosky, A., Munroe, P., 2009. Physical Properties of Biochar, in:
1031 Lehmann, J., Joseph, S. (Eds.), Biochar for Environmental Management: Science
1032 and Technology. Earthscan, London, pp. 13–32.
1033 Drizo, A., Forget, C., Chapuis, R.P., Comeau, Y., 2006. Phosphorus removal by electric
1034 arc furnace steel slag and serpentinite. Water Res. 40, 1547–1554.
1035 doi:10.1016/j.watres.2006.02.001
1036 Enders, A., Lehmann, J., 2012. Comparison of Wet-Digestion and Dry-Ashing Methods
1037 for Total Elemental Analysis of Biochar. Commun. Soil Sci. Plant Anal. 43, 1042–
1038 1052. doi:10.1080/00103624.2012.656167
1039 Fang, L., Huang, L., Holm, P.E., Yang, X., Hansen, H.C.B., Wang, D., 2015. Facile
1040 upscaled synthesis of layered iron oxide nanosheets and their application in
1041 phosphate removal. J. Mater. Chem. A 3, 7505–7512. doi:10.1039/C4TA07083F
1042 Goldberg, S., Sposito, G., 1985. On the mechanism of specific phosphate adsorption by
1043 hydroxylated mineral surfaces: A review. Commun. Soil Sci. Plant Anal. 16, 801–
1044 821. doi:10.1080/00103628509367646
1045 Greenop, R., Wentworth, J., 2014. Phosphate Resources. UK Parliamentary Office of
1046 Science and Technology. POSTnote 477.
1047 Gull, M., Zhou, M., Fernández, F.M., Pasek, M.A., 2014. Prebiotic phosphate ester
1048 syntheses in a deep eutectic solvent. J. Mol. Evol. 78, 109–117.
1049 doi:10.1007/s00239-013-9605-9
1050 Hale, S.E., Alling, V., Martinsen, V., Mulder, J., Breedveld, G.D., Cornelissen, G.,

2013. The sorption and desorption of phosphate-P, ammonium-N and nitrate-N in cacao shell and corn cob biochars. Chemosphere 91, 1612–1619. doi:10.1016/j.chemosphere.2012.12.057

Heller-Kallai, L., Miloslavski, I., Aizenshtat, Z., Halicz, L., 1988. Chemical and mass spectrometric analysis of volatiles derived from clays. Am. Mineral. 73, 376–382.

Hollister, C.C., Bisogni, J.J., Lehmann, J., 2013. Ammonium, Nitrate, and Phosphate Sorption to and Solute Leaching from Biochars Prepared from Corn Stover (Zea mays L.) and Oak Wood (Quercus spp.). J. Environ. Qual. 42, 137–44. doi:10.2134/jeq2012.0033

IBI, 2012. Standardized Product Definition and Product Testing Guidelines for Biochar That Is Used in Soil. International Biochar Initiative (IBI).

Joseph, S., Graber, E.R., Chia, C., Munroe, P., Donne, S., Thomas, T., Nielsen, S., Marjo, C., Rutlidge, H., Pan, G., Li, L., Taylor, P., Rawal, A., Hook, J., 2013. Shifting paradigms: development of high-efficiency biochar fertilizers based on nano-structures and soluble components. Carbon Manag. 4, 323–343. doi:10.4155/cmt.13.23

Laird, D., Rogovska, N., 2015. Biochar Effects on Nutrient Leaching, in: Lehmann, J., Joseph, S. (Eds.), Biochar for Environmental Management, Science, Technology and Implementation. Routledge, Oxon, pp. 521–542.

Li, J., Lv, G., Bai, W., Liu, Q., Zhang, Y., Song, J., 2016. Modification and use of biochar from wheat straw (Triticum aestivum L.) for nitrate and phosphate removal from water. Desalin. Water Treat. 57, 4681–4693. doi:10.1080/19443994.2014.994104

Littler, J., Geroni, J.N., Sapsford, D.J., Coulton, R., Griffiths, A.J., 2013. Mechanisms of phosphorus removal by cement-bound ochre pellets. Chemosphere 90, 1533–

1538. doi:10.1016/j.chemosphere.2012.08.054

Magdziarz, A., Wilk, M., 2013. Thermal characteristics of the combustion process of biomass and sewage sludge. J. Therm. Anal. Calorim. 114, 519–529. doi:10.1007/s10973-012-2933-y

Mallet, M., Barthélémy, K., Ruby, C., Renard, A., Naille, S., 2013. Investigation of phosphate adsorption onto ferrihydrite by X-ray Photoelectron Spectroscopy. J. Colloid Interface Sci. 407, 95–101. doi:10.1016/j.jcis.2013.06.049

Morales, M.M., Comerford, N., Guerrini, I. a., Falcão, N.P.S., Reeves, J.B., 2013. Sorption and desorption of phosphate on biochar and biochar-soil mixtures. Soil Use Manag. 29, 306–314. doi:10.1111/sum.12047

Mukherjee, A., Zimmerman, A.R., Harris, W., 2011. Surface chemistry variations among a series of laboratory-produced biochars. Geoderma 163, 247–255. doi:10.1016/j.geoderma.2011.04.021

Namasivayam, C., Sangeetha, D., 2004. Equilibrium and kinetic studies of adsorption of phosphate onto ZnCl2 activated coir pith carbon. J. Colloid Interface Sci. 280, 359–65. doi:10.1016/j.jcis.2004.08.015

Onay, O., Kockar, O.M., 2003. Slow, fast and flash pyrolysis of rapeseed. Renew. Energy 28, 2417–2433. doi:10.1016/S0960-1481(03)00137-X

Parfitt, R., 1989. Phosphate reactions with natural allophane, ferrihydrite and goethite. J. Soil Sci. 40, 359–369. doi:10.1111/j.1365-2389.1989.tb01280.x

Parfitt, R.., Russell, J.., 1977. Adsorption on hydrous oxides. IV. mechanisms of adsorption of various ions on goethite. J. Soil Sience 28, 297–305.

Parfitt, R.L., Atkinson, R.J., Smart, R.S.C., 1975. The Mechanism of Phosphate Fixation by Iron Oxides. Soil Sci. Soc. Am. 39, 838–841. doi:10.2136/sssaj1975.03615995003900050017x

1101 Park, J.H., Ok, Y.S., Kim, S.H., Cho, J.S., Heo, J.S., Delaune, R.D., Seo, D.C., 2015.
1102 Evaluation of phosphorus adsorption capacity of sesame straw biochar on aqueous
1103 solution: influence of activation methods and pyrolysis temperatures. Environ.
1104 Geochem. Health 37, 969–983. doi:10.1007/s10653-015-9709-9
1105 Qiu, Y., Zheng, Z., Zhou, Z., Sheng, G.D., 2009. Effectiveness and mechanisms of dye
1106 adsorption on a straw-based biochar. Bioresour. Technol. 100, 5348–5351.
1107 doi:10.1016/j.biortech.2009.05.054
1108 Rawal, A., Joseph, S.D., Hook, J.M., Chia, C.H., Munroe, P.R., Donne, S.W., Lin, Y.,
1109 Phelan, D., Richard, D., Mitchell, G., Pace, B., Horvat, J., Beau, J., Webber, W.,
1110 2016. Mineral-Biochar Composites: Molecular Structure and Porosity. Environ.
1111 Sci. Technol. 50, 7706–7714. doi:10.1021/acs.est.6b00685
1112 Reddy, K.R., Kadlec, R.H., Flaig, E., Gale, P.M., 1999. Phosphorus retention in streams
1113 and wetlands: a review. Crit. Rev. Environ. Sci. Technol. 29, 83–146.
1114 doi:10.1080/10643389991259182
1115 Reijnders, L., 2014. Resources , Conservation and Recycling Phosphorus resources ,
1116 their depletion and conservation , a review. "Resources, Conserv. Recycl. 93, 32–
1117 49. doi:10.1016/j.resconrec.2014.09.006
1118 Ren, J., Li, N., Li, L., An, J.-K., Zhao, L., Ren, N.-Q., 2015. Granulation and ferric
1119 oxides loading enable biochar derived from cotton stalk to remove phosphate from
1120 water. Bioresour. Technol. 178, 119–125. doi:10.1016/j.biortech.2014.09.071
1121 RStudio Team, 2015. RStudio: Integrated Development for R.
1122 Sakadevan, K., Bavor, H.J., 1998. Phosphate adsorption characteristics of soils, slags
1123 and zeolite to be used as substrates in constructed wetland systems. Water Res. 32,
1124 393–399. doi:10.1016/S0043-1354(97)00271-6
1125 Schneider, F., Haderlein, S.B., 2016. Potential effects of biochar on the availability of

1126 phosphorus — mechanistic insights. Geoderma 277, 83–90.
1127 doi:10.1016/j.geoderma.2016.05.007
1128 Shepherd, J.G., Sohi, S.P., Heal, K.V., 2016. Optimising the recovery and re-use of
1129 phosphorus from wastewater effluent for sustainable fertiliser development. Water
1130 Res. 94, 155–165. doi:10.1016/j.watres.2016.02.038
1131 Sibrell, P.L., Montgomery, G. a., Ritenour, K.L., Tucker, T.W., 2009. Removal of
1132 phosphorus from agricultural wastewaters using adsorption media prepared from
1133 acid mine drainage sludge. Water Res. 43, 2240–2250.
1134 doi:10.1016/j.watres.2009.02.010
1135 Silber, A., Levkovitch, I., Graber, E.R., 2010. PH-dependent mineral release and surface
1136 properties of cornstraw biochar: Agronomic implications. Environ. Sci. Technol.
1137 44, 9318–9323. doi:10.1021/es101283d
1138 Steenari, B., Lindqvist, O., 1998. High Temperature Reactions of Straw Ash and the
1139 Anti-Sintering Additives Kaolin and Dolomite. Biomass and Bioenergy 14, 67–76.
1140 Steffen, W., Richardson, K., Rockström, J., Cornell, S., Fetzer, I., Bennett, E., Biggs,
1141 R., Carpenter, S.R., de Wit, C. a., Folke, C., Mace, G., Persson, L.M.,
1142 Veerabhadran, R., Reyers, B., Sörlin, S., 2015. Planetary Boundaries: Guiding
1143 human development on a changing planet. Science 347.
1144 doi:10.1126/science.1259855
1145 Streubel, J.D., Collins, H.P., Tarara, J.M., Cochran, R.L., 2012. Biochar Produced from
1146 Anaerobically Digested Fiber Reduces Phosphorus in Dairy Lagoons. J. Environ.
1147 Qual. 41, 1166. doi:10.2134/jeq2011.0131
1148 Torrent, J., Schwertmann, U., Barrón, V., 1992. Fast and slow phosphate sorption by
1149 goethite-rich natural materials. Clays Clay Miner. 40, 14–21.
1150 doi:10.1346/CCMN.1992.0400103

1151 Wang, Z., Nie, E., Li, J., Yang, M., Zhao, Y., Luo, X., Zheng, Z., 2012. Equilibrium
1152 and kinetics of adsorption of phosphate onto iron-doped activated carbon. Environ.
1153 Sci. Pollut. Res. 19, 2908–2917. doi:10.1007/s11356-012-0799-y
1154 Yao, Y., Gao, B., Inyang, M., Zimmerman, A.R., Cao, X., Pullammanappallil, P., Yang,
1155 L., 2011. Biochar derived from anaerobically digested sugar beet tailings:
1156 Characterization and phosphate removal potential. Bioresour. Technol. 102, 6273–
1157 6278. doi:10.1016/j.biortech.2011.03.006
1158 Yao, Y., Gao, B., Zhang, M., Inyang, M., Zimmerman, A.R., 2012. Effect of biochar
1159 amendment on sorption and leaching of nitrate, ammonium, and phosphate in a
1160 sandy soil. Chemosphere 89, 1467–1471. doi:10.1016/j.chemosphere.2012.06.002
1161 Zhang, H., Chen, C., Gray, E.M., Boyd, S.E., Yang, H., Zhang, D., 2016. Roles of
1162 biochar in improving phosphorus availability in soils: A phosphate adsorbent and a
1163 source of available phosphorus. Geoderma 276, 1–6.
1164 doi:10.1016/j.geoderma.2016.04.020
1165 Zhang, M., Gao, B., Yao, Y., Inyang, M., 2013. Phosphate removal ability of
1166 biochar/MgAl-LDH ultra-fine composites prepared by liquid-phase deposition.
1167 Chemosphere 92, 1042–1047. doi:10.1016/j.chemosphere.2013.02.050
1168 Zhang, M., Gao, B., Yao, Y., Xue, Y., Inyang, M., 2012. Synthesis of porous MgO-
1169 biochar nanocomposites for removal of phosphate and nitrate from aqueous
1170 solutions. Chem. Eng. J. 210, 26–32. doi:10.1016/j.cej.2012.08.052
1171